

Review

Two-Dimensional Materials for Dendrite-Free Zinc Metal Anodes in Aqueous Zinc Batteries

Wen Xu ^{1,†}, Minghui Zhang ^{1,†}, Yanfeng Dong ^{1,*}  and Jingwen Zhao ^{2,3,*} ¹ Department of Chemistry, College of Sciences, Northeastern University, Shenyang 110819, China² Qingdao Industrial Energy Storage Research Institute, Qingdao Institute of Bioenergy and Bioprocess Technology, Chinese Academy of Sciences, Qingdao 266101, China³ Shandong Energy Institute, Qingdao 266101, China

* Correspondence: dongyanfeng@mail.neu.edu.cn (Y.D.); zhaojw@qibebt.ac.cn (J.Z.)

† These authors contributed equally to this work.

Abstract: Aqueous zinc batteries (AZBs) show promising applications in large-scale energy storage and wearable devices mainly because of their low cost and intrinsic safety. However, zinc metal anodes suffer from dendrite issues and side reactions, seriously hindering their practical applications. Two-dimensional (2D) materials with atomic thickness and large aspect ratio possess excellent physicochemical properties, providing opportunities to rationally design and construct practically reversible zinc metal anodes. Here, we systematically summarize the recent progress of 2D materials (e.g., graphene and MXene) that can be used to enable dendrite-free zinc metal anodes for AZBs. Firstly, the construction methods and strategies of 2D materials/Zn hybrid anodes are briefly reviewed, and are classified into protecting layers on Zn foils and host materials for Zn. Secondly, various 2D material/Zn hybrid anodes are elaborately introduced, and the key roles played by 2D materials in stabilizing the Zn/Zn²⁺ redox process are specially emphasized. Finally, the challenges and perspectives of advanced 2D materials for advanced Zn anodes in next-generation AZBs are briefly discussed.



Citation: Xu, W.; Zhang, M.; Dong, Y.; Zhao, J. Two-Dimensional Materials for Dendrite-Free Zinc Metal Anodes in Aqueous Zinc Batteries. *Batteries* **2022**, *8*, 293. <https://doi.org/10.3390/batteries8120293>

Academic Editors: Junnan Hao, Long Zhang and Seung-Wan Song

Received: 24 October 2022

Accepted: 16 December 2022

Published: 19 December 2022

Publisher's Note: MDPI stays neutral with regard to jurisdictional claims in published maps and institutional affiliations.



Copyright: © 2022 by the authors. Licensee MDPI, Basel, Switzerland. This article is an open access article distributed under the terms and conditions of the Creative Commons Attribution (CC BY) license (<https://creativecommons.org/licenses/by/4.0/>).

Keywords: 2D materials; aqueous zinc batteries; zinc metal anode

1. Introduction

Aqueous zinc batteries (AZBs) are deemed as promising next-generation battery technology for wearable devices and large-scale energy storage applications [1–6], which is mainly ascribed to several advantages of zinc metal anodes, such as low electrochemical potential (−0.76 V vs. SHE) [7–10], high hydrogen evolution reaction overpotential, and low cost. During the past decade, great efforts have been made to improve the conductivity of cathode materials and inhibit the cathode dissolution in mild electrolytes [11–13]. Unfortunately, notorious zinc dendrite issues and side reactions (e.g., hydrogen evolution reaction and corrosion reaction) in traditional aqueous electrolytes seriously deteriorate the reversibility of zinc metal anodes, which has been recognized as a major obstacle to construct high-performance AZBs [14–18].

To address the above challenges, two effective strategies, including protecting layers on Zn [19–23], and advanced host materials for Zn [24–26], have been frequently employed [12,27–30]. For example, a nitrogen-doped, graphene (NG)-based protecting layer on a Zn anode could achieve dendrite-free Zn deposition with (002) plane orientation; therefore, the resulting NG/Zn-based symmetrical cell could exhibit 600 and 150 cycles at 1 and 5 mA cm^{−2} [31], respectively. Notably, two-dimensional (2D) materials with atomic thickness and large aspect ratio possess excellent physicochemical properties; specifically, graphene nanosheets possess excellent mechanical flexibility, a high theoretical specific surface area (SSA) of 2630 m² g^{−1}, and superior electrical conductivity of 107 S m^{−1} [32–41]. In addition, MXene nanosheets have abundant surface functional

groups (e.g., -F, -O, -Cl), good electrical conductivity of $60\text{--}80\text{ S m}^{-1}$, high Young's modulus up to 0.33 TPa, and a fast ion diffusion coefficient [42–44]. Remarkably, 2D materials can be easily assembled into macroscopical films or aerogels, which can be further employed as protecting layers on Zn or host materials for Zn. For example, MXene nanosheets were assembled on Zn anodes, and the resulting hybrid anodes exhibited improved ion transport kinetics, and suppressed Zn dendrites and side reactions; thus, excellent electrochemical performance was achieved, such as a high capacity retention of 81% after 500 cycles (1 A g^{-1}), and a low voltage hysteresis of 47 mV (0.2 mA cm^{-2}) [43,45]. As another typical example, when covalent organic framework (COF) films with ultrathin thicknesses of 10–200 nm and a large area were coated on Zn anodes, they could preclude the formation of by-products and homogenize the Zn deposition; as a result, symmetrical Zn cells delivered an extended cycling life of 400 h at 1 mA cm^{-2} and 1 mAh cm^{-2} [46]. However, the rational design and construction of 2D material-based protecting layers on Zn or host materials for AZBs remain challenging, which is mainly caused by the poor contact between 2D materials and metal Zn, and limited zincophilic sites [1,47–53]. Therefore, it is timely and necessary to systematically review the recent progress of 2D materials for Zn metal anodes, and summarize the lessons to provide valuable and objective guidelines that will be valuable for designing more advanced zinc metal anodes for AZBs [54–57].

Herein, the recent progress of dendrite-free zinc metal anodes enabled by 2D materials (e.g., graphene, MXene and other 2D materials) in AZBs is systematically reviewed. Firstly, we summarize common construction strategies of 2D material/Zn hybrid anodes. Then, various 2D materials/Zn hybrid anodes are specially elaborated to demonstrate the enhanced electrochemical performance caused by the presence of 2D materials (Figure 1). Finally, challenges and prospects of 2D materials for high-performance reversible Zn anodes in the next-generation AZBs are briefly discussed.

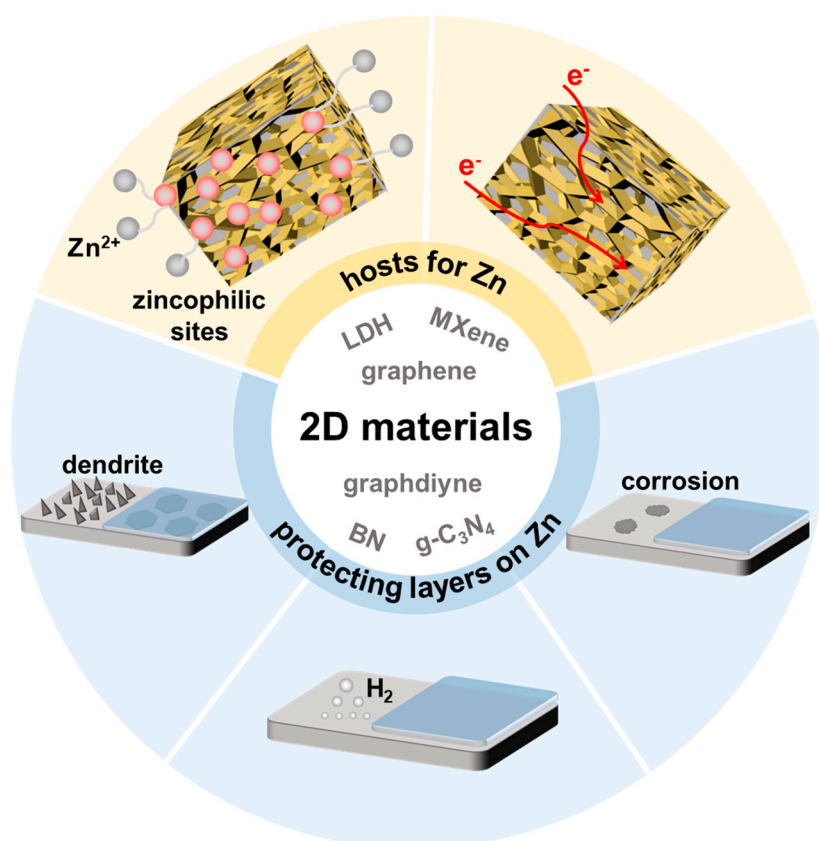


Figure 1. Schematic of 2D materials for Zn metal anodes in high-performance AZBs.

2. Construction Strategies of 2D Material/Zn Hybrid Anodes

Various 2D materials possess unique physicochemical properties; however, the severe agglomeration of 2D materials usually occurs because of the Van der Waals' force and, correspondingly, their excellent properties cannot be fully exploited. Therefore, it is of great importance to adopt suitable strategies to construct 2D material/Zn hybrid anodes in order to maximize the function of 2D materials. Common construction strategies mainly include blade coating, the Langmuir-Blodgett method and dipping coating, electrochemical deposition, three-dimensional (3D) printing, and other methods, which will be elaborately introduced in this section.

2.1. Blade Coating

The blade coating method is frequently used for constructing protecting layers on Zn anodes because of its easy operation, which generally involves two steps. The selected 2D material is firstly mixed with an appropriate amount of binder in suitable solvents to prepare uniform slurry; subsequently, the slurry is uniformly blade-coated on the surface of zinc foils. After drying, the targeted 2D material/Zn hybrids can be obtained. Using such a facile method, the thickness of the protecting layers can be easily controlled via changing the viscosity of the employed slurry or the space between the blade and the substrate surface. Notably, the non-aqueous binders (e.g., polyvinylidene fluoride (PVDF)) are normally dissolved into N-methylpyrrolidone (NMP) solvent. For example, Hao et al. mixed NG and PVDF in an NMP solvent with a mass ratio of 9:1, and the resulting slurry was coated on Zn foil, resulting in an NG-based artificial protective layer on Zn anode [58]. Similarly, Li et al. blended MXene nanosheets with PVDF under a mass ratio of 95:5 in NMP solvent, and then, the resulting slurry was blade-coated on pre-cleaned Zn foil [59]. In addition, graphene oxide (GO)-modified 2D boron nitride (BN) was selected to mix with PVDF in an NMP solvent to evenly coat the Zn foil surface by means of a scraper after continuous ultrasonic agitation [60]. As for aqueous binders, water is commonly selected as the disperse solvent. For instance, Zhou et al. ultrasonically treated GO powder, a water binder, and water to prepare GO-based slurry for Zn anode coating [61]. Moreover, N-richened surfactant-polydiallyldimethylammonium chloride (PDDA) was added into an alkalinized $Ti_3C_2T_x$ MXene colloidal solution to disperse selenium powder (Se), giving birth to a $Ti_3C_2T_x$ MXene@PDDA@Se ink, which could be directly coated on the surface of Zn foils [62]. Furthermore, chitosan was selected as a strong chelator to mix with MXene suspension with a mass ratio of 1:5 to obtain a uniform and viscous suspension, which was further coated on a Zn foil (Figure 2a) [63]. As another example, coating and polymerization were integrated into a single step simultaneously; specifically, 2-acrylamido-2-methylpropanesulfonic acid (AMPS) powder and acrylic acid (AA) can be polymerized in an ice bath to generate P(AA-co-AMPS) hydrogel. When MXene nanosheets were added in the reaction system, the P(AA-co-AMPS)-MXene hydrogel could be obtained, and based on such a principle, the P(AA-co-AMPS)-MXene hydrogel could be directly coated and formed on zinc foil [64]. Such a strategy is facile and facilitates the intimate interface between P(AA-co-AMPS)-MXene and Zn metal.

2.2. Langmuir-Blodgett Method and Dipping Coating

Both the Langmuir-Blodgett method and dipping coating methods can achieve ultrathin films on the target substrate. In the case of the typical Langmuir-Blodgett method, amphiphilic molecules with both hydrophilic and hydrophobic functional groups disperse at the liquid/air interface, and gradually gather together to form a monomolecular layer; subsequently, such an ultrathin layer can be transferred onto the target substrate. For instance, NG dispersion in ethanol was added into water, and NG could be evenly spread on the upper surface of water, generating a thin NG-based film. When Zn foil was pulled out of the solution, NG could spontaneously coat on the Zn foil (Figure 2b) [31]. The dipping coating method is another commonly used method to construct protecting coatings on Zn anodes. Especially benefitting from the potential differences between the modifying

materials and metal zinc, the 2D materials can be spontaneously and uniformly deposited on Zn foils when they are pulled from the immersion solution, and the thickness of the 2D material-based protecting layers can be easily controlled by the concentration of 2D materials and dipping coating times. Not limited to graphene, MXene nanosheets can also be intimately deposited on Zn foils based on similar principles, and the amount of deposited MXene nanosheets on Zn foil can be regulated by simply adjusting the reaction time or the MXene concentration of the immersion solution [45,65].

2.3. Electrochemical Deposition

Electrochemical deposition is a facile and safe strategy to construct 2D material/Zn hybrid anodes, in which 2D materials are usually employed as one electrode, and Zn salts (e.g., ZnSO_4) are dissolved in the electrolytes, and when an electric field is applied, Zn^{2+} ions are reduced to Zn at the electrolyte/electrode. When porous host electrodes are employed, 2D material/Zn hybrid anodes with high SSA can be obtained. Therefore, such electrochemical deposition is frequently employed to construct 2D material based host/Zn hybrid anodes. For a typical example, Wu et al. used graphene-like carbon film (GCF), Pt foil, and Ag/AgCl as the working electrode, counter electrode, and reference electrode [66], respectively, and metallic zinc was electrochemically deposited onto GCF in a solution of 0.2 M ZnSO_4 and 0.5 M $\text{Na}_3\text{C}_6\text{H}_5\text{O}_7 \cdot 2\text{H}_2\text{O}$, giving rise to the Zn@GCF hybrid anodes. In addition, Zn foils can be directly employed as the electrode substrate with the precursors of targeted 2D materials existing in electrolytes. When a certain electrical field is applied, due to the guide of the electrical field, 2D materials usually show vertical orientation on Zn substrates. For example, Sanket prepared Zn@MoS₂ by using a three-electrode system with a Zn working electrode, Pt counter electrode, Ag/AgCl reference electrode, and 5 mM ammonium tetrathiomolybdate as the electrolyte (Figure 2c) [67]. Notably, during the process of electrodeposition, heterogeneous nucleation and subsequent growth behaviors determine the final structures of electrodeposited zinc.

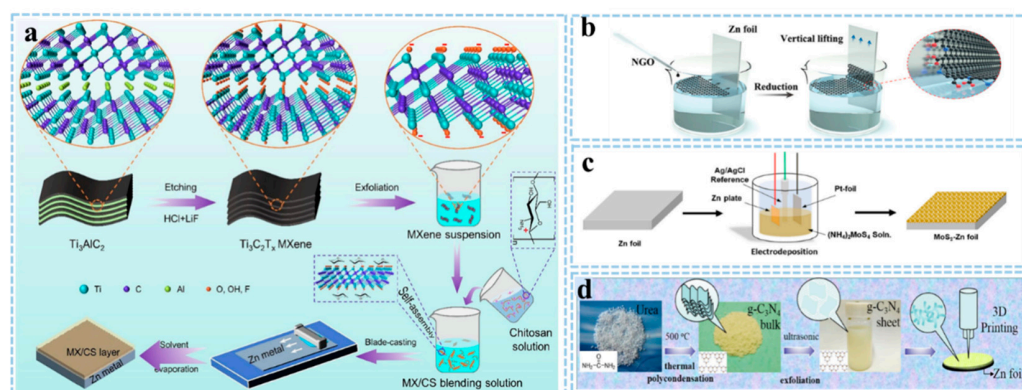


Figure 2. Construction strategies for 2D material/Zn hybrid anodes. (a) blade coating, reproduced with permission from Ref. [63] Copyright 2022, Elsevier. (b) Langmuir-Blodgett and dipping coating, reproduced with permission from Ref. [31] Copyright 2021, Wiley-VCH. (c) electrochemical deposition, reproduced with permission from Ref. [67] Copyright 2020, American Chemical Society. (d) 3D printing, reproduced with permission from Ref. [68] Copyright 2021, Elsevier.

2.4. 3D Printing

3D porous electrodes allow ions to diffuse in random directions, facilitating faster reaction kinetics than bulk counterparts; in this regard, 3D printing is an effective technique to customize desired 3D structures for high-performance AZBs, and the advantages of such a method includes customization of complex architectures and precise control of an electrode's shape and thickness. As a typical example, urea was employed to prepare $\text{g-C}_3\text{N}_4$ mainly via a polycondensation reaction and ultrasonic peeling, and the as-fabricated $\text{g-C}_3\text{N}_4$ -based ink could be 3D printed on the surface of a zinc anode (Figure 2d) [68].

Importantly, the printed g-C₃N₄ layer could play a significant role in realizing the uniform deposition of zinc. Notably, the key to 3D printing is the successful fabrication of 2D material-based inks with suitable viscosity and surface tension; so far, only graphene and MXene-based inks have been reported for 3D printing. Obviously, in the near future, other 2D materials will be ready to be exploited for 3D printing ink and further application in advanced Zn metal anodes.

2.5. Other Methods

Apart from the mentioned approaches, other methods have also been developed to achieve the application of 2D materials in high-performance Zn anodes. Specifically, when 2D materials are used as the host for metallic Zn, fast ion transport in a 2D direction can be ensured; meanwhile, rich surface functional groups or atoms of 2D materials can be used as zincophilic sites to lower the nucleation barrier energy and induce homogeneous zinc deposition. Mechanically rolling or pressing ductile Zn metal with 2D materials under external pressure is the most direct way to employ 2D materials as Zn hosts. For example, zinc foam was firstly immersed into a GO solution, and GO nanosheets were reduced to graphene oxide (rGO) by Zn to fill in the large pores of Zn [69]. Subsequently, the resulting hybrid foam was mechanically compressed under a pressure of 8 MPa; thus graphene interpenetrated Zn (GiZn) hybrid foils were obtained and, notably, the robust GiZn could ensure the intimate interactions between graphene and Zn and avoid the falling off of graphene, demonstrating the superiority of such a method for advanced Zn anodes.

3. Application of 2D Materials in Zn Anodes

As we mentioned above, zinc metal anodes have attracted great attention for AZBs because of their high hydrogen evolution overpotential and suitable redox potential [36,70–72]. However, unlimited growth of zinc dendrites and side reactions between Zn and aqueous electrolytes usually result in low Coulombic efficiency and undesirable cycling life, seriously hindering their commercial applications. In this regard, 2D materials with ultra-thin thickness and excellent properties can be employed to guide uniform Zn-ion flux via physical or chemical effects when they are employed as protecting layers on Zn metal anodes, and local current density can be reduced when 2D materials are employed as advanced Zn hosts with high SSA. With the consideration of so many choices of 2D materials (e.g., graphene, MXene), advanced 2D material/Zn hybrid anodes can be expected to achieve desirable electrochemical performance. In addition, to better compare the differences of various 2D materials and electrodes, various 2D material/Zn hybrid anodes and their key electrochemical performances are summarized in Table 1.

Table 1. A summary of various reported 2D material/Zn hybrid anodes.

Type of 2D Material	Anode Name	Voltage Hysteresis	Nucleation Overpotential	Life Span	Average CE	Refs.
Graphene	Zn@PG	58 mV (1 mA cm ⁻²)	40 mV	400 h (1 mA cm ⁻²)	97.37%/100	[73]
	Zn@rGO	–	~20 mV	300 h (1 mA cm ⁻²)	–	[74]
	FLG@Zn	69 mV (1 mA cm ⁻²)	54 mV	500 h (1 mA cm ⁻²)	98%/100	[75]
	NG@Zn	37.2 mV (1 mA cm ⁻²)	84.3 mV	500 h (1 mA cm ⁻²)	–	[58]
	NGO@Zn	17 mV (1 mA cm ⁻²)	–	1200 h (1 mA cm ⁻²)	99.5%/250	[31]
	MZn	–	11 mV	2000 h (0.5 mA cm ⁻²)	–	[76]
	PEDOT:PSS/GS@Zn	–	66 mV	500 h (1 mA cm ⁻²)	98%/100	[77]
	ZGL@Zn	42 mV	108 mV	>2180 h (0.5 mA cm ⁻²)	99.6%/1450	[78]
	GiZn	30.4 mV (0.5 mA cm ⁻²)	35 mV	792 h (0.5 mA cm ⁻²)	96.8%/200	[69]
	Zn/GCF	–	–	100 h (1 mA cm ⁻²)	~100%/100	[66]
GQDs	50 mV (0.8 mA cm ⁻²)	36.5 mV	2200 h (0.8 mA cm ⁻²)	–	[79]	

Table 1. Cont.

Type of 2D Material	Anode Name	Voltage Hysteresis	Nucleation Overpotential	Life Span	Average CE	Refs.
MXene	Ti ₃ C ₂ T _x MXene@Zn	75 mV (1 mA cm ⁻²)	–	300 h (1 mA cm ⁻²)	94.13%/400	[80]
	ZnGaIn//MXene	25 mV (1 mA cm ⁻²)	~0 mV	600 h (1 mA cm ⁻²)	–	[81]
	MCF@Zn	63 mV (10 mA cm ⁻²)	14 mV	300 h (10 mA cm ⁻²)	97.72%/500	[82]
	LF-MXene	63 mV (5 mA cm ⁻²)	32 mV	280 h (5 mA cm ⁻²)	–	[83]
	MXene@Sb	–	–	1000 h (0.5 mA cm ⁻²)	97.2%/1500	[84]
	MZn	47 mV (0.2 mA cm ⁻²)	16 mV	>800 h (0.2 mA cm ⁻²)	–	[45]
	Ti ₃ C ₂ Cl ₂ .Zn	<103 mV (2 mA cm ⁻²)	40.7 mV	>840 h (2 mA cm ⁻²)	99.3%/200	[59]
	S/MX@ZnS@Zn	27 mV (1 mA cm ⁻²)	–	1100 h (1 mA cm ⁻²)	–	[85]
	N/Se-MXene@ZnSe@Zn	35 mV (1 mA cm ⁻²)	20 mV	2500 h (1 mA cm ⁻²)	–	[62]
	MX-TMA@Zn	~60 mV (2 mA cm ⁻²)	–	3600 h (2 mA cm ⁻²)	–	[65]
Other 2D materials	MX/CS@Zn	76 mV (0.5 mA cm ⁻²)	31 mV	2100 h (1 mA cm ⁻²)	>99%/500	[63]
	PASM-Zn	–	–	>1900 h (0.2 mA cm ⁻²)	–	[64]
	MXene-mPPy/Zn	29 mV (1 mA cm ⁻²)	10 mV	2500 h (0.2 mA cm ⁻²)	–	[86]
	BN@Zn	25.4 mV (1 mA cm ⁻²)	27 mV	3000 h (1 mA cm ⁻²)	99.3%/150	[87]
	BNNFs@Zn	51 mV (1 mA cm ⁻²)	–	1600 h (1 mA cm ⁻²)	–	[88]
	S-BN@Zn	45 mV	26 mV	2500 h (2 mA cm ⁻²)	99.5%/60	[89]
	MoS ₂ @Zn	–	120 mV	>150 h (2.5 mA cm ⁻²)	–	[67]
	LDH@Zn	37.7 mV (1 mA cm ⁻²)	–	400 h (1 mA cm ⁻²)	99.2%/2000	[90]
	g-C ₃ N ₄ @Zn	80 mV (2 mA cm ⁻²)	~55 mV	500 h (2 mA cm ⁻²)	–	[68]
	GDY@Zn	25 mV (4 mA cm ⁻²)	–	>400 h (4 mA cm ⁻²)	98%/200	[91]

FLG: a few layers of graphene; MCF: MXene-modified copper foam; GQDs: graphene quantum dots; MZn: MXene-coated Zn; BNNFs: porous boron nitride nanofibers; S-BN: sulfonate-modified boron nitride nanosheets; GDY: graphdiyne.

3.1. Graphene for Zn Anodes

Graphene possesses a large theoretical SAA and 2D ultrathin structure, greatly facilitating fast Zn ion transfer and parallel growth of Zn flakes caused by the crystal match between graphene and (002) Zn. Importantly, graphene nanosheets can be grafted with abundant functional groups, which can act as zincophilic sites to induce uniform Zn deposition. In addition, graphene is also employed as a conductive host material for Zn, reducing local current density and improving the electrical conductivity of the hybrid anodes [92,93]. In the following content, typical examples of graphene/Zn hybrid anodes will be elaborated to demonstrate the unique roles of graphene for advanced Zn anodes.

Graphene-based coating layers play a crucial role in inhibiting zinc dendrite growth by providing abundant zincophilic sites and regulating uniform Zn-ion flux [94]. Moreover, the thickness of the coating layers also determines the energy barriers for Zn²⁺ ion transport kinetics. For instance, Du et al. mixed pristine graphene (PG) with Zn for the synthesis of hybrid anode (PG@Zn), in which Zn particles were well adhesive enough to integrate with each other into one electrode without the help of adhesives (Figure 3a) [73]. As a result, the notorious zinc dendrite issue was well solved since horizontal zinc flakes were evenly deposited due to the matched hexagonal lattice structures between PG and Zn. Compared with Zn foil-based symmetric cells with a cycle life of 70 h, Zn@PG based symmetric cells could cycle steadily for more than 400 h (1 mA cm⁻²) (Figure 3b), which is superior to most reported Zn anodes (Figure 3c). Another outstanding advantage of the Zn@PG anode is the low mass loading and high utilization of Zn; correspondingly, the whole battery showed a high energy density of 80 Wh kg⁻¹, which is twice than that of a pure Zn anode. Meanwhile, a high rate capacity of 240 mA g⁻¹ (1 A g⁻¹) was also achieved. Such an anode design integrates well with graphene nanosheets with Zn particles (instead of traditional Zn foils), demonstrating the promising application of graphene nanosheets for flexible and high-energy-density AZBs.

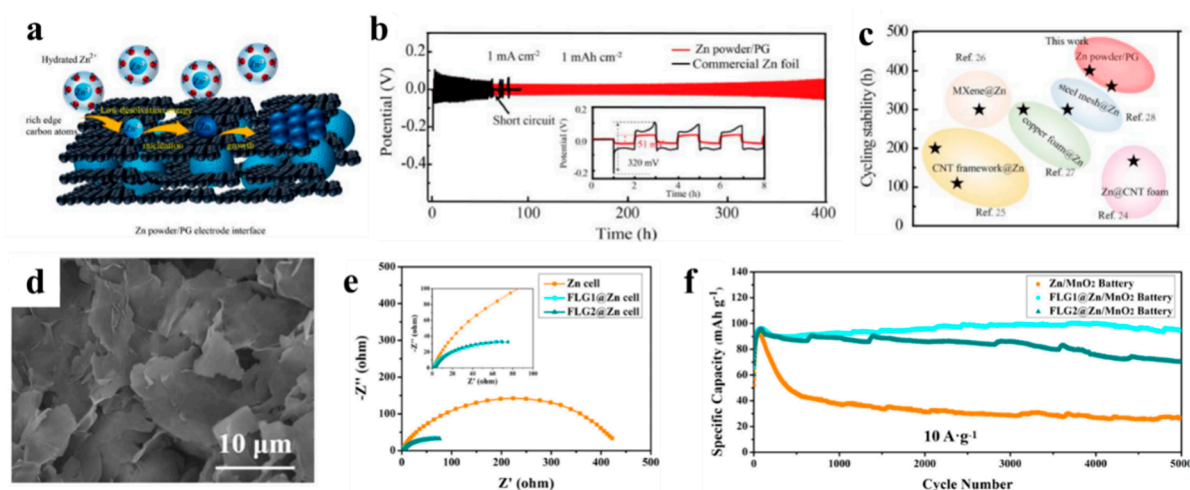


Figure 3. (a) The schematic diagram of the Zn deposition progress on Zn@PG. (b) Long-term cycling performance of Zn@PG||Zn@PG and Zn||Zn symmetric cells at 1 mA cm^{-2} . (c) A comparison of electrochemical performance between Zn@PG symmetric cells and reported anodes. Reproduced with permission from Ref. [73] Copyright 2022, Elsevier. (d) SEM image of FLG. (e) EIS curves of Zn||Zn and FLG@Zn||FLG@Zn symmetrical cells. (f) Cycling performance of Zn/MnO₂ and FLG@Zn/MnO₂ cells at 10 A g^{-1} . Reproduced with permission from Ref. [75] Copyright 2022, Wiley-VCH.

Not limited to PG, GO nanosheets were also employed to modify Zn metal anodes. Compared with a pure Zn anode, the GO-modified Zn exhibited faster transfer kinetics, reduced the zinc dissolution problem in mild acid electrolyte, and greatly improved Zn utilization [61]. It was worth noting that the optimal electrochemical performance was achieved when GO accounted for 1.92 wt.% of the total anode mass. In contrast to the bare Zn anode, the impedance of a GO-coated Zn electrode in its electrochemical impedance spectroscopy (EIS) was significantly reduced. Moreover, GO nanosheets were spontaneously reduced by Zn, and the resulting rGO nanosheets uniformly distributed on the surface of Zn, and greatly promoted the uniform Zn-ion flux for even Zn deposition [74]. Moreover, the thickness of the rGO layer could be adjusted by the Zn soaking time in GO suspension; correspondingly, the voltage hysteresis of Zn@rGO anode varied. Notably, the cycled Zn@rGO anode still maintained a smooth surface after 100 cycles, and in sharp contrast, obvious dendrites could be observed in the case of bare Zn anodes. Importantly, the Zn@rGO anode enabled the assembled full battery to stably cycle 2000 times with a high capacity retention of 88%. With the consideration of the rich surface chemistry of GO as well as its low cost, we believe that GO will play an increasingly important role in constructing advanced Zn metal anodes.

Notably, the thicknesses of the protecting layers on Zn anodes can significantly influence the final electrochemical performance. For instance, FLG with few functional groups was beneficial to reduce the energy barrier for zinc ion transport and homogenize zinc ions uniformly [75]. Subsequently, the FLG was sprayed onto a Zn anode to prepare FLG@Zn hybrid anodes (Figure 3d). Importantly, the impedance of a FLG@Zn-based symmetric cell was only 150Ω (Figure 3e), obviously smaller than that of the pure Zn based counterpart. Moreover, the FLG@Zn-based Zn/MnO₂ batteries delivered a high capacity retention of 97% after 5000 cycles at 10 A g^{-1} (Figure 3f).

To provide more active sites to regulate Zn deposition, NG was effectively synthesized via annealing the graphene in an NH₃ atmosphere [58]. Notably, the nitrogen species were beneficial to interact with Zn ions for uniform Zn-ion flux; meanwhile, the nuclear barrier of the NG@Zn-based symmetric cell was only 84.3 mV, much smaller than that of the bare Zn-based counterpart (139.8 mV). In addition, Chen and co-workers prepared a nitrogen-doped graphene oxide (NGO) coating layer using the Langmuir-Blodgett method (Figure 4a) [31], and the thickness of the NGO layer could be easily adjusted by varying the

concentration of precursor solution. Importantly, the NGO@Zn symmetric cell exhibited a stable cycling life of 1200 h at 1 mA cm^{-2} (Figure 4b), and the capacity retention of the NGO@Zn-based full battery was 94% after 300 cycles at 0.5 C (Figure 4c), indicating the unique roles of NGO for enhanced electrochemical performance. Theoretically, other heteroatom doping (e.g., S, P, and B) can play similar roles, which is ready to be confirmed by experimental results in the future.

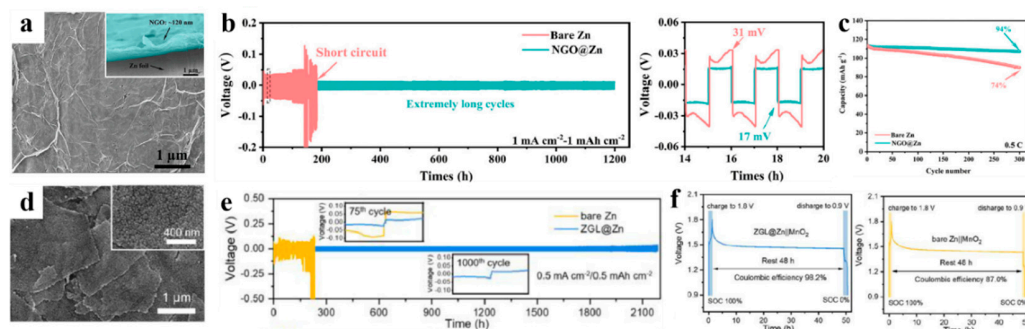


Figure 4. (a) The SEM illustration of the surface of NGO; long-term cycling performance of (b) NGO@Zn||NGO@Zn and Zn||Zn symmetric cells at 1 mA cm^{-2} and (c) LMO||Zn and LMO||NGO@Zn full cells at 0.5 C. Reproduced with permission from Ref. [31] Copyright 2021, Wiley-VCH. (d) SEM image of the surface of ZGL. (e) Voltage profiles of pristine Zn and ZGL@Zn symmetric cell at 0.5 mA cm^{-2} . (f) Self-discharge curves of the Zn||MnO₂ and ZGL@Zn||MnO₂ cells. Reproduced with permission from Ref. [78] Copyright 2022, Elsevier.

To further widen the functionalities of the graphene-based protecting layers on Zn, other functional materials were also selected to modify the graphene nanosheets. For example, a bilayer composite consisting of a copper nanosheet and GO nanosheets was synthesized, and subsequently coated on the surface of the Zn anode [76]. The as-fabricated hybrid possessed several advantages. Firstly, the poor conductivity of GO avoided possible side reactions between the Zn and the electrolyte. Secondly, copper nanosheets not only enhanced ion transfer kinetics, but also reduced the nucleation barrier. Consequently, the modified Zn-based symmetric cells achieved an ultra-long stable cycle of 2000 h, which is 10 times longer than that of pure Zn. Importantly, the modified Zn endowed an AZB full battery with a high capacity retention of 86% after 600 cycles at 1 A g^{-1} , significantly higher than that of pure Zn (59%). Conductive polymers were also employed as hybrids with graphene; for instance, conductive poly(3,4-ethylenedioxythiophene)-poly(Styrenesulfonate) (PEDOT:PSS) was electrochemically deposited on graphene nanosheets (GSs) [77] to synthesize the PEDOT:PSS/GS hybrid, and the presence of PEDOT:PSS greatly improved the conductivity of the hybrid electrodes and lowered the polarization. Consequently, when PEDOT:PSS/GS was coated on Zn, the resulting hybrid anode (PEDOT:PSS/GS@Zn) endowed the corresponding symmetric battery with a cycling life of 500 h, obviously longer than the bare Zn-based counterpart (85 h), and the as-assembled PEDOT:PSS/GS@Zn||MnO₂ battery displayed an impressive cycle life of 8000 h at 1 A g^{-1} . Furthermore, Prasit and co-workers coated polypyrrole/rGO composites (PPy/rGO) on Zn surfaces [95]. Specifically, PPy had a better wetting ability than its inorganic counterparts, facilitating fast Zn-ion diffusion kinetics. As a result, when PPy/rGO was coated on a Zn anode, the resulting hybrid anode (Zn-PPy/rGO) endowed the corresponding symmetric cell with a voltage hysteresis of 25 mV, which is much smaller than the value of a Zn||Zn symmetric cell (89 mV). Importantly, the Zn-PPy/rGO||MnO₂ battery exhibited a high initial discharge capacity of 325 mAh g^{-1} at 0.5 A g^{-1} and a capacity retention of 50% after 300 cycles. Moreover, GO nanosheets were firstly modified by a zeolitic imidazolate framework (ZIF-8) (Figure 4d); subsequently, with the help of PVDF, a multifunctional protective layer (ZGL) was built on Zn foil [78]. Specifically, the presence of a ZGL layer could isolate zinc from the electrolyte to a large extent, effectively avoiding the occurrence of side reactions. Therefore, no dendrites and by-products could be observed in

the as-fabricated ZGL@Zn||ZGL@Zn symmetric cell; importantly, the symmetric cell exhibited a cycling life of over 2000 h at 0.5 mA cm^{-2} , longer than the control cell with bare Zn (150 h) (Figure 4e). In addition, the ZGL@Zn||MnO₂ full battery displayed an anti-self-discharge ability (Figure 4f), as evidenced by 98% of the original voltage after a rest time of 48 h, higher than that of the Zn||MnO₂ cell (87%). Despite the great progress of graphene-based hybrids for Zn metal anodes, the synergistic effects between graphene and its modification have not yet revealed; therefore, in the future, more efforts should be exerted to screen the best modification material and disclose the mentioned synergistic effects for enhanced electrochemical performance.

Not limited to protecting layers, graphene-based materials can act as advanced hosts for Zn [78]. As a typical example, rGO nanosheets were firstly assembled on the Zn skeletons, and then, the obtained hybrid was subjected to mechanical compression for the synthesis of graphene-interpenetrated zinc anode materials (GiZn) [69]. Specifically, rGO not only provided zincophilic sites, but also induced homogeneous Zn deposition. Consequently, GiZn-based symmetrical cells exhibited enhanced Zn electrochemical performance, such as a low voltage hysteresis of 30.4 mV and a high areal capacitance of 30 mAh cm^{-2} at 0.5 mA cm^{-2} . Meanwhile, the as-fabricated GiZn||MnO₂ cathodes delivered a specific capacity of 168 mAh g^{-1} at 8 C, much higher than that of the counterpart with pure Zn anodes (72 mAh g^{-1}). Furthermore, Wu et al. firstly synthesized GCF from graphite paper using the electrochemical intercalation method [66], and the GCF possessed a unique 2D-3D hybrid grid, and thus could work as conductive hosts for Zn. Therefore, Zn was electrochemically deposited on GCF to prepare Zn/GCF hybrid anodes. Importantly, the assembled AZBs displayed high capacities of 381.8 and 379 mAh g^{-1} at 100 and 3000 mA g^{-1} , respectively, demonstrating the unique roles of GCF for advanced AZBs.

In addition, graphene can be used as an electrolyte additive to optimize the electrochemical performance of a Zn anode. For example, GQDs with abundant oxygen-containing functional groups in electrolytes were conducive to bind with Zn²⁺ ions, promoting uniform Zn deposition of Zn [79]. As a result, GQDs were endowed with the as-assembled AZBs with a high capacity retention of 70% at 0.5 A g^{-1} after 500 cycles, higher than the value of the counterpart without GQDs (58%). Such pioneer works may enlighten researchers to rationally design advanced electrolytes with 2D material-based additives.

3.2. MXene for Zn Anodes

MXene possesses excellent conductivity and hydrophilicity, and the presence of MXene nanosheets on Zn foils may improve the anode/electrolyte interface, distribute the Zn-ion flux, and provide abundant zincophilic sites to induce dendrite-free Zn deposition [96–98]. Notably, MXene nanosheets with high aspect ratio can be assembled into porous films or aerogels, which could be further employed as hosts for Zn deposition, effectively avoiding the excessive Zn in traditional Zn foil anodes with low energy density. When MXene nanosheet-based coating layers are chosen to modify the Zn anode surface, rapid ion and electron transfers could be simultaneously ensured; moreover, the direct contact between the electrolyte and Zn is effectively prevented, physically inhibiting the growth of dendrite and the occurrence of corrosion reactions. In the following section, MXene hosts for Zn and MXene coatings on Zn will be elaborated in detail.

3.2.1. MXene Hosts for Zn

As we mentioned above, MXene nanosheets can be assembled into flexible papers without auxiliary materials and employed as advanced hosts for Zn. For example, after a Zn plating time of 20 h, the as-fabricated MXene||Zn hybrid anode (Ti₃C₂T_x MXene@Zn) maintained a smooth surface without obvious protrusions and filaments [80]. Importantly, the Ti₃C₂T_x MXene@Zn||Zn asymmetric battery achieved a high Coulombic efficiency of 100% after 400 cycles at 5 mA cm^{-2} . Furthermore, MXene film was selected as a substrate for zinc-enriched liquid metal (ZnGaIn) loading, in which metal indium could act as the nucleation sites to induce uniform Zn deposition [81]; correspondingly, the

nucleation barrier of Zn was greatly reduced. Specifically, compared with the nucleation overpotentials of MXene (10 mV), Al foil (39 mV), Ti foil (43 mV), and Zn foil (46 mV), the fabricated ZnGaIn//MXene anode showed negligible nucleation overpotential at 0.1 mA cm^{-2} (Figure 5a). Impressively, the ZnGaIn//MXene also showed excellent flexibility, and no capacity decay could be observed for the bent ZnGaIn//MXene-based symmetric cells (Figure 5b), demonstrating their promising application in flexible devices.

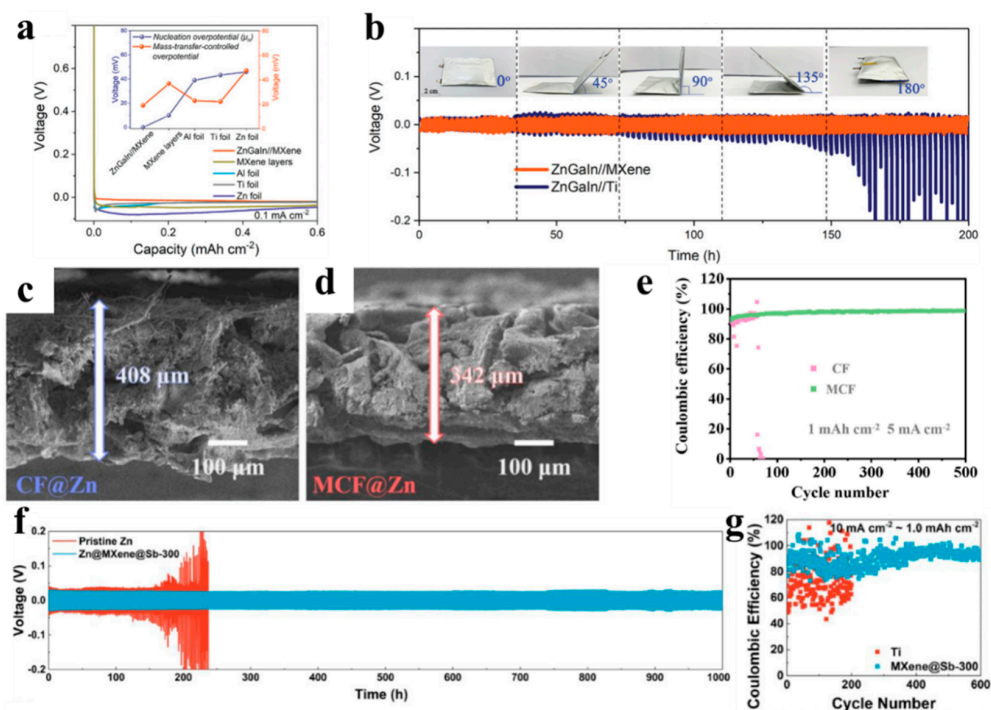


Figure 5. (a) Nucleation overpotential of Zn deposition on ZnGaIn//MXene and other foils at 0.1 mA cm^{-2} . (b) Voltage profiles of ZnGaIn//MXene and ZnGaIn//Ti symmetric cells at different bending angles, reproduced with permission from Ref. [81] Copyright 2022, Wiley-VCH. Cross-sectional SEM images of (c) cycled CF@Zn and (d) MCF@Zn. (e) Coulombic efficiencies of Zn|CF and Zn|MCF half cells at 5 mA cm^{-2} and 1 mAh cm^{-2} , reproduced with permission from Ref. [82] Copyright 2022, Elsevier. (f) Long-term cycling performance of Zn@MXene/Sb||Zn@MXene/Sb and Zn||Zn symmetric cells at 0.5 mA cm^{-2} and 0.5 mA h cm^{-2} . (g) Coulombic efficiencies of Zn||MXene/Sb and Zn||Ti cells at 10 mA cm^{-2} and 1 mAh cm^{-2} , reproduced with permission from Ref. [84] Copyright 2021, Elsevier.

MXene nanosheets are also applied as modified layers on current collectors/hosts to induce dendrite-free Zn deposition. As a typical example, MXene nanosheets were firstly employed to modify copper foam (CF), and the corresponding hybrid (MCF) could provide abundant Zn nucleation sites and homogenize Zn-ion flux [82]. Furthermore, after Zn deposition, the thickness of the resulting MCF@Zn hybrid anode ($342 \mu\text{m}$) was obviously thinner than that of CF@Zn electrode ($408 \mu\text{m}$) (Figure 5c,d), indicating that volume expansion of electrodes during charge/discharge cycles was effectively alleviated. Furthermore, with the help of MCF, an average Coulombic efficiency of 97.72% could be achieved at 5 mA cm^{-2} (Figure 5e). In addition, functional groups of MXene can significantly influence the final electrochemical performance. For example, when MXene nanosheets with less F-contained function groups were deposited on Zn foils, MXene could effectively accelerate Zn^{2+} ion transfer and homogenize local current distribution and nucleation sites; interestingly, the horizontal growth of Zn with a flat surface was achieved at 2.5 mAh cm^{-2} . Importantly, the resulting hybrid anode could achieve a cycling life of 280 h with a low voltage hysteresis of 63 mV at 5 mA cm^{-2} and 5 mAh cm^{-2} [83]. Those advances demonstrate the superiority of MXene nanosheets for high-performance Zn

anodes well; however, the chemical stability of MXene nanosheets should not be ignored since MXene nanosheets tend to be oxidized to corresponding metal oxides; meanwhile, the conductivities of MXene nanosheets decrease rapidly.

Some anti-corrosive metals (e.g., Cu, Sb) were also reported as composites with MXene to synergistically inhibit side reactions between the Zn and the electrolyte. For instance, MXene paper was employed as a Zn host, and Sb was introduced into the hybrid anode, which could be used in-situ to transform the ZnSb phase during the Zn deposition process; as a result, the assembled symmetrical cell could operate for 1000 h (0.5 mA cm^{-2} and 0.5 mAh cm^{-2}) and 500 h (5 mA cm^{-2} and 5 mAh cm^{-2}) (Figure 5f) [84], respectively. Benefitting from the synergistic effect between antimony and MXene, the MXene@Sb||Ti electrode guaranteed a cycling life of 600 times with good Coulombic efficiencies at 10 mA cm^{-2} (Figure 5g). In the future, the feasibilities of other anti-corrosive metal/MXene hybrids are ready to be evaluated for dendrite-free zinc anodes.

3.2.2. MXene Coatings on Zn

Not limited to MXene-based hosts for Zn, MXene nanosheets are frequently applied as protecting layers on Zn foils to greatly improve the wettability of electrolyte/electrode interfaces, and homogenize the dispersion of Zn-ion flux for uniform Zn deposition. For example, the Zn foils with an MXene coating (MZn) exhibited better electrolyte wettability than pure Zn, and a long cycling life of 800 h with a low voltage hysteresis of 47 mV at 0.2 mA cm^{-2} could be achieved, indicating the key roles of MXene in promoting uniform Zn-ion flux and electric field distribution [45]. In addition, function groups on MXene nanosheets greatly influence the functions of MXene-based protecting layers. For instance, MXene nanosheets with different halogen function groups ($\text{Ti}_3\text{C}_2\text{Cl}_2$, $\text{Ti}_3\text{C}_2\text{Br}_2$ and $\text{Ti}_3\text{C}_2\text{I}_2$) were employed as coating layers on Zn [54], and $\text{Ti}_3\text{C}_2\text{Cl}_2$ MXene could achieve homogeneous Zn deposition and promote the formation of a coherent non-uniform Zn-MXene interface to restrain Zn dendrites; therefore, the $\text{Ti}_3\text{C}_2\text{Cl}_2$ -Zn-based symmetric battery delivered a cycling life of 840 h at 2 mA cm^{-2} , which is about 13 times longer than of its counterpart with bare Zn (65 h).

To provide more zincophilic sites, heteroatoms are frequently introduced to MXene nanosheets. For instance, since sulfur or selenium can react with Zn to produce ZnS or ZnSb nanoparticles with high ionic conductivity, sulfur-doped MXene nanosheets were coated on a Zn anode, and ZnS was generated in-situ, resulting in the highly reversible and dendrite-free hybrid anode (S/MX@ZnS@Zn) [85]. Importantly, the S/MX@ZnS@Zn-based symmetric cell exhibited a lower polarization of 27 mV and longer cycling life of 1100 h (1.0 mA cm^{-2} and 1.0 mAh cm^{-2}) than that of the Zn foil-based counterpart (Figure 6a). Benefitting from the synergistic effect between ZnS and MXene, a relatively smooth surface was observed even under a high Zn deposition capacity of 20 mAh cm^{-2} (Figure 6b). Further, N and Se co-doped MXene-based protecting layers on Zn foils (N/Se-MXene@ZnSe@Zn) were also reported to enhance the hydrophilicity of Zn metal, and the in-situ formed ZnSe nanoparticles acted as abundant zincophilic sites to improve the reversibility of the Zn anode [62]. Importantly, the N/Se-MXene@ZnSe@Zn hybrid anode-based symmetric battery exhibited better electrochemical performance than pristine Zn, as evidenced by a long cycle life over 2500 h and a low polarization of 23 mV at 1.0 mA cm^{-2} and 1.0 mAh cm^{-2} . Moreover, tetramethylammonium (TMA) with nitrogen-containing functional groups was intercalated into $\text{Ti}_3\text{C}_2\text{T}_x$ MXene, and when the MXene (MX-TMA) was coated on a Zn anode, the resulting MX-TMA@Zn anode facilitated rapid Zn ion diffusion and enhanced electrochemical performance [65]. In this regard, other heteroatoms doped or intercalated MXene as protective layers for Zn anode are expected to demonstrate equally excellent performance.

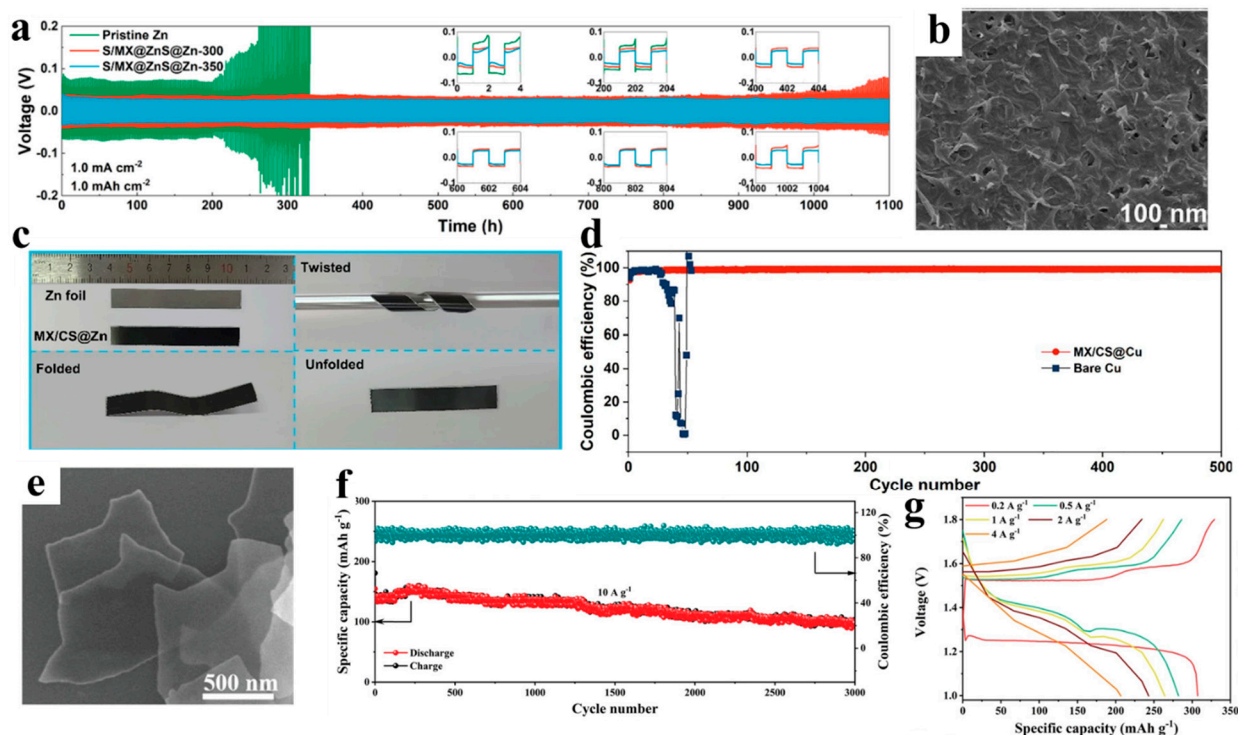


Figure 6. (a) Long-time cycling performance of S/MX@ZnS@Zn and Zn symmetric cells at 1.0 mA cm^{-2} and 1.0 mAh cm^{-2} . (b) SEM image of S/MX@ZnS@Zn anode, reproduced with permission from Ref. [85] Copyright 2021, American Chemical Society. (c) Photographs of MX/CS@Zn foils with different states. (d) Coulombic efficiencies of the Zn||Cu cells at 0.5 mA cm^{-2} , reproduced with permission from Ref. [63] Copyright 2022, Elsevier. (e) SEM image of MXene-mPPy nanosheets. (f) Electrochemical stability of MXene-mPPy/Zn||MnO₂ battery at 10 A g^{-1} . (g) Charge/discharge curves of MXene-mPPy at different current densities from 0.2 to 4 A g^{-1} , reproduced with permission from Ref. [86] Copyright 2022, Wiley-VCH.

To improve the interfacial contact between MXene-based layers and Zn foils, polymers are also employed to composites with MXene nanosheets. For example, a protective layer (MX/CS) consisting of MXene and chitosan showed extraordinary fastness between MX/CS and Zn foil even under folding and twisting conditions (Figure 6c) [63]. Meanwhile, a long cycling life of 2100 h and low polarization of 100 mV could be achieved at 1 mA cm^{-2} in MX/CS@Zn-based symmetric cells, and a high Coulombic efficiency of 99% was maintained after 500 cycles in the MX/CS@Zn||Cu battery (Figure 6d). Notably, the aggregation of MXene usually occurs during the MXene coating on Zn. In this regard, the rapid polymerization of monomer in an aqueous solution is an effective method to avoid the above circumstance. For instance, acrylic acid and 2-acrylamido-2-methylpropanesulfonic acid reacted in the presence of MXene for the synthesis of P(AA-co-AMPS)-MXene, which was then coated on Zn foil (PASM-Zn) [64]. Notably, a Zn^{2+} transference number ($t_{\text{Zn}^{2+}}$) of 0.21 was achieved in bare Zn; in sharp contrast, the $t_{\text{Zn}^{2+}}$ increased to 0.49 in the case of PASM-Zn, indicating that the transport of Zn ions tended to be near the adsorption site rather than along the interface; thus the concentration gradient was reduced, further promoting the ion transport kinetics; therefore, respectable electrochemical performance was achieved, such as a long cycling life of 1900 h and 900 h at 0.2 and 1 mA cm^{-2} . In addition, the PAMS-Zn||NaV₃O₈·1.5H₂O battery also showed high capacity retentions of 86.2% and 85.0% after 1000 and 2600 cycles, respectively. To improve the electrical conductivity of the MXene/polymer hybrids, conductive polymers (e.g., polypyrrole) are ideal choices. The artificial layer of the MXene-based mesoporous polypyrrole (MXene-mPPy) on a Zn anode could effectively homogenize Zn-ion flux (Figure 6e); correspondingly, the MXene-mPPy/Zn symmetric battery exhibited a long service life up to 2500 h at 0.2 mA cm^{-2} ,

superior to its counterparts with polypyrrole/Zn and pure Zn [86]. Notably, the presence of abundant mesopores greatly facilitated the uniform concentration gradient near the Zn anode; thereby, a high capacity of 307 mAh g^{-1} at 0.2 A g^{-1} and a long-term cycling life over 3000 times (10 A g^{-1}) were achieved (Figure 6f,g), demonstrating the promising application of MXene-mPPy/Zn for high-performance AZBs.

3.3. Other 2D Materials for Zn Anodes

In addition to the aforementioned graphene and MXene, other 2D materials (e.g., BN, MoS_2 , $\text{g-C}_3\text{N}_4$) have also been reported for zinc metal anodes. Those 2D materials mainly show inferior conductivity to graphene and MXene, but display other unique physicochemical properties (e.g., high mechanical stiffness and semiconductor properties); thus, such 2D material-based protecting layers on Zn foils can physically distribute Zn-ion flux and inhibit Zn dendrites, penetrating separators. Meanwhile, the crystal match between 2D materials and metal Zn may guide the horizontal Zn deposition. As a typical example, BN was physically vapor-deposited onto Zn foil for the synthesis of BN@Zn electrodes [87]. Importantly, the thickness of the BN film could be precisely controlled in a nanoscale range. With the help of in-situ optical microscopy, obvious dendrites could be visually observed on the surface of cycled Zn; in sharp contrast, the surface of BN@Zn remained flat and smooth. Correspondingly, the activation energy of BN@Zn was determined to be 37.2 KJ mol^{-1} , much lower than the value of Zn (67.8 KJ mol^{-1}), indicating the key roles of the BN layer in reducing de-solvation energy. Importantly, the BN@Zn|| MnO_2 battery could be cycled steadily for 3000 h at 1 A g^{-1} , longer than that of a Zn|| MnO_2 cell (2000 h). Furthermore, porous BN nanofibers (BNNFs) with negatively charged surfaces were coated on Zn anodes for the synthesis of BNNFs@Zn anodes, in which the uniform Zn-ion flux could be achieved via chemical coordination between BNNFs and Zn^{2+} ions [88]. Consequently, the BNNFs@Zn-based symmetric cells could cycle stably for 500 h at a high current density of 10 mA cm^{-2} , which was about three times longer than that of the Zn-based symmetric cells. In addition, the BNNFs@Zn endowed the corresponding full battery with an initial capacity of 293 mAh g^{-1} at 1 A g^{-1} and a high capacity retention of 97% after 400 cycles. Moreover, sodium dodecylbenzenesulfonate (SDBS) was employed to modify boron nitride, and the resulting sulfonate-modified boron nitride (S-BN) nanosheets were further spray-coated on Zn foils (Figure 7a) [89]. Notably, the strong interaction between the sulfonate group and Zn^{2+} ions greatly facilitated ion mobility. Meanwhile, the presence of S-BN could greatly suppress the corrosion reaction of Zn. Therefore, the corrosion potential of S-BN@Zn was as low as -0.986 V , which is smaller than that of bare Zn (-0.993 V). Meanwhile, the S-BN@Zn electrode displayed a smaller nucleation overpotential of 26 mV, greater than bare Zn (112 mV) (Figure 7b). When the current density was increased to 1 A g^{-1} , and the S-BN@Zn-based full battery displayed a long-term cycling life of 1000 times, which was obviously longer than the counterpart with a bare Zn anode (100 cycles) (Figure 7c).

As another kind of functional material, 2D transition metal sulfides can also enhance the reversibility of Zn anodes. For example, Sanket et al. electrochemically deposited vertical 2D MoS_2 on Zn anodes (MoS_2 @Zn) [67], in which MoS_2 greatly facilitated the diffusion of zinc ions and uniform electric field distribution near the electrode. In a chronoamperometry test, the current-time graph of the MoS_2 @Zn electrode was relatively stable and showed no significant increase compared with the Zn electrode, indicating the limited 2D diffusion for uniform Zn deposition (Figure 7d). At the same time, the MoS_2 @Zn electrode showed lower series resistance than the Zn electrode in an EIS test (Figure 7e), indicating enhanced electrochemical kinetics. As a result, the AZBs with MoS_2 @Zn anodes achieved a capacity of 150 mAh g^{-1} at 1 A g^{-1} and a long cycling life of 2000 h; in contrast, the counterpart with a bare Zn anode failed only after 750 h (Figure 7f).

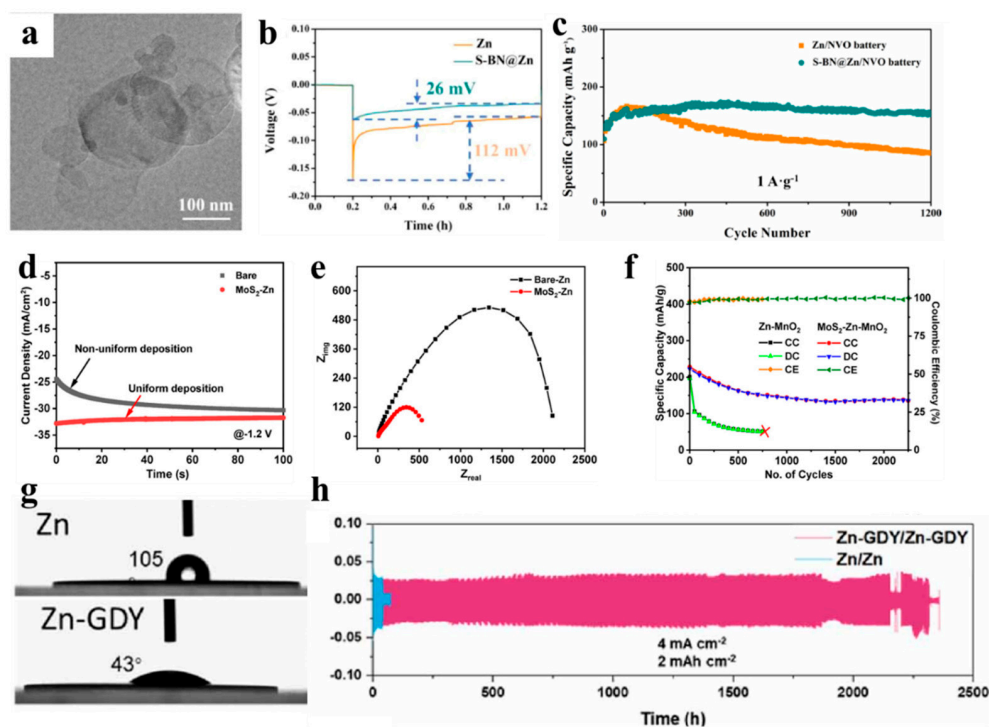


Figure 7. (a) TEM image of S-BN. (b) Nucleation overpotentials of bare Zn and S-BN@Zn electrodes at $1 \text{ mA} \cdot \text{cm}^{-2}$. (c) Long-term cycling performance of S-BN@Zn||NVO and Zn||NVO batteries at $1 \text{ A} \cdot \text{g}^{-1}$, reproduced with permission from Ref. [89] Copyright 2021, Elsevier. (d) Current density vs. time profiles of Zn and $\text{MoS}_2\text{-Zn}$ electrodes. (e) EIS curves of Zn and $\text{MoS}_2\text{-Zn}$ -based symmetrical cells after 10 cycles. (f) Cycling performance of a Zn- MnO_2 battery using $\text{MoS}_2\text{-Zn}$ anodes at $1 \text{ A} \cdot \text{g}^{-1}$, reproduced with permission from Ref. [67] Copyright 2020, American Chemical Society. (g) Contact angles of Zn and Zn-GDY electrodes. (h) Cycling performance of Zn||Zn and Zn-GDY||Zn-GDY symmetric cells at $4 \text{ mA} \cdot \text{cm}^{-2}$, reproduced with permission from Ref. [91] Copyright 2021, IOP Publishing.

In addition, layered double hydroxides (LDHs) are also important functional 2D materials, and can be employed to construct solid electrolyte interface (SEI) films for Zn anode protection. For instance, Mg-Al LDH (Mg-Al LDH) displays superior stability and insulation features, and the appropriate layer spacing of Mg-Al LDH can act as ion channels, and the presence of Mg-Al LDH can also alleviate the dissolution of the Zn anode in an acid electrolyte [90]. By analyzing the polarization curves, the Zn anode with an LDH coating layer (LDH@Zn) only showed a corrosion current density of $0.2 \text{ mA} \cdot \text{cm}^{-2}$, which is one-fifth of the value of the bare Zn electrode, demonstrating the anti-corrosion ability of the LDH-based protecting layer. Meanwhile, the polarization of the LDH@Zn-based symmetric cell is 65 mV at $2 \text{ mA} \cdot \text{cm}^{-2}$, lower than that of the Zn-based counterpart (78 mV). Importantly, the assembled LDH@Zn|| MnO_2 battery exhibited better cycling performance, as evidenced by a capacity retention of 75% after 400 cycles at $1 \text{ A} \cdot \text{g}^{-1}$, higher than that of the control battery with a bare Zn anode ($\sim 35\%$).

As another important functional material, semiconductive $g\text{-C}_3\text{N}_4$ nanosheets possess high N content and a suitable band gap when the $g\text{-C}_3\text{N}_4$ -based protecting layer was constructed on Zn via 3D printing technology [68]. The unique porous structure and defects of $g\text{-C}_3\text{N}_4$ nanosheets facilitated the Zn ion transfer. Notably, the interaction between Zn^{2+} ions and N species of $g\text{-C}_3\text{N}_4$ nanosheets induced a homogeneous distribution of Zn-ion flux. Density functional theory further disclosed that the binding energy of $g\text{-C}_3\text{N}_4$ and Zn^{2+} ion was -1.24 eV , and potential-current density analysis showed that the $g\text{-C}_3\text{N}_4\text{@Zn}$ electrode had a lower overpotential than the Zn electrode. Most importantly, the $g\text{-C}_3\text{N}_4\text{@Zn}$ -based full battery showed a cycling life over 500 h at $1 \text{ A} \cdot \text{g}^{-1}$ and a high capacity retention of 94%, which is significantly higher than the bare Zn-based counterpart (84%).

As a new carbon nanomaterial, graphdiyne (GDY) possesses unique pore structures and excellent electrical conductivity, which can be directly synthesized on Zn metal substrates [99]. As a typical example, Zhang and co-workers synthesized GDY films with the help of a radio frequency generator [91]. Notably, the contact angle between GDY@Zn and water was only 43° , which is much smaller than that of bare Zn and water (105°), indicating improved hydrophilicity (Figure 7g). Importantly, the GDY@Zn displayed negligible capacity decay over 95 cycles, whereas in the case of bare Zn anode, obvious capacity decay was observed within 20 cycles. Meanwhile, the GDY@Zn-based symmetric battery cycled stably for more than 2000 h at 4 mA cm^{-2} , obviously longer than that of the control cell with a bare Zn anode ($\sim 50 \text{ h}$) (Figure 7h).

4. Conclusions and Prospects

In summary, we systematically summarized the research progress of 2D materials (e.g., graphene, MXene, BN, g-C₃N₄) for Zn metal anodes in high-performance AZBs. Firstly, the construction strategies of 2D material/Zn hybrid anodes were briefly introduced. Secondly, the enhanced electrochemical performance of various 2D material/Zn hybrid anodes were elaborated, highlighting the unique roles of 2D materials in protecting layers on Zn and host materials for Zn. Although significant progress has been made in this field, some challenges and opportunities of 2D material/Zn hybrid anodes coexist, which can be summarized as follows:

- (1) New strategies remain to be developed to precisely construct ultra-thin and stable 2D material-based protecting layers on Zn. At present, 2D materials are usually mixed with polymer binders, and then coated on Zn foils to construct 2D material/Zn hybrid anodes, in which the thickness of protecting layers is relatively thick. Meanwhile, the interfaces between the protecting layers and Zn anodes are usually weak, seriously deteriorating their cycling stability. In this regard, physical vapor deposition and atomic layer deposition may be the feasible strategies since the deposition time and other parameters can be precisely controlled, and the interfaces between deposited films and substrates are intimate [100]. Moreover, other advanced strategies can also be considered, such as 3D printing [101,102], magnetron sputtering [87,103,104], and laser etching.
- (2) To fabricate flexible and wearable battery devices, it is indispensable to construct Zn host materials with high mechanical strength and innocuous and zincophilic features. In this regard, some 2D materials can be ideal materials for Zn anode supports. However, the research on 2D material-based hosts for Zn is still in its infancy, because only graphene and MXene nanosheets have been reported to serve as Zn host materials so far. Therefore, other 2D materials with unique physicochemical properties are highly needed to be exploited and evaluated their potentials for high-performance Zn metal anodes in the near future; in this regard, controllable synthesis and assembly of 2D materials with desirable structures and properties (e.g., flexibility) are of great importance to construct flexible AZBs.
- (3) Two-dimensional material/Zn hybrid anodes should be evaluated in harsh conditions for practical applications. At present, most reported works on 2D materials for Zn anodes conduct electrochemical tests under gentle conditions. To meet the requirements of practical application, 2D material/Zn hybrid anodes should be evaluated in harsh conditions, such as high-capacity Zn deposition, high areal current density, and even extreme temperatures. In this regard, 2D materials will definitely play key roles in improving the reversibility of Zn anodes under such harsh conditions since it is feasible to rationally select one 2D material with specific properties from the large pool of candidates.
- (4) Advanced characterizations are highly needed to understand the real roles of 2D materials for enhanced electrochemical performance. The understanding of the mechanism of Zn dendrite formation is still in the initial stage. The issues of Zn dendrite formation and HER can be suppressed at the source only by truly exploring the root causes of

them. Therefore, advanced technologies (e.g., in situ synchrotron radiation and spherical aberration-corrected electron microscope) are needed to insightfully disclose the structural evolution of 2D materials, the interfacial interactions between 2D materials and Zn, and the mechanisms of 2D materials on the de-solvation behaviors of Zn^{2+} ions. Meanwhile, theoretical calculations and simulations should be combined to better understand the relative results in terms of thermodynamic and dynamic views.

In summary, with the development of the controllable preparation technology of existing 2D materials and the exploitation of new 2D material systems, we believe that 2D materials play a momentous role in realizing practically feasible high-performance Zn anodes. Lastly, AZBs require different components (cathodes, anodes, and electrolytes) to work cooperatively to achieve excellent electrochemical performance; with the consideration of the great progress of cathodes and electrolytes, practical AZBs are expected to be realized in the near future.

Author Contributions: Conceptualization, Y.D., W.X., M.Z. and J.Z.; writing—original draft preparation, W.X. and M.Z.; writing—review and editing, Y.D., W.X., M.Z. and J.Z.; supervision, Y.D. and J.Z.; project administration, Y.D. and J.Z.; funding acquisition, Y.D. and J.Z. All authors have read and agreed to the published version of the manuscript.

Funding: This work was funded by Liaoning Revitalization Talents Program (XLYC2007129), the Natural Science Foundation of Liaoning Province (2020-MS-095), the Fundamental Research Funds for the Central Universities of China (N2105008), the National Natural Science Foundation of China (Grant No. 21975271), the fund of the State Key Laboratory of Catalysis in DICP (N-21-03), the Major Basic Research Projects of Shandong Natural Science Foundation (ZR2020ZD07), the Shandong Energy Institute (Grant No. SEI I202127), and the Youth Innovation Promotion Association of CAS (2019214).

Institutional Review Board Statement: Not applicable.

Informed Consent Statement: Not applicable.

Data Availability Statement: Not applicable.

Conflicts of Interest: The authors declare no conflict of interest.

References

1. Liu, J.; Xia, H.; Xue, D.F.; Lu, L. Double-Shell Nanocapsules of V_2O_5 -Based Composites as High-Performance Anode and Cathode Materials for Li Ion Batteries. *J. Am. Chem. Soc.* **2009**, *131*, 12086–12087. [[CrossRef](#)]
2. Liu, Z.X.; Huang, Y.; Huang, Y.; Yang, Q.; Li, X.L.; Huang, Z.D.; Zhi, C.Y. Voltage issue of aqueous rechargeable metal-ion batteries. *Chem. Soc. Rev.* **2020**, *49*, 180–232. [[CrossRef](#)]
3. Dong, Y.; Miao, L.C.; Ma, G.Q.; Di, S.L.; Wang, Y.Y.; Wang, L.B.; Xu, J.B.; Zhang, N. Nonconcentrated aqueous electrolytes with organic solvent additives for stable zinc batteries. *Chem. Sci.* **2021**, *12*, 5843–5852. [[CrossRef](#)]
4. Chao, D.L.; Zhou, W.H.; Ye, C.; Zhang, Q.H.; Chen, Y.G.; Gu, L.; Davey, K.; Qiu, S.Z. An Electrolytic Zn-MnO₂ Battery for High-Voltage and Scalable Energy Storage. *Angew. Chem. Int. Ed.* **2019**, *58*, 7905–7910. [[CrossRef](#)]
5. Xue, H.R.; Gong, H.; Yamauchi, Y.; Sasaki, T.; Ma, R.Z. Photo-enhanced rechargeable high-energy-density metal batteries for solar energy conversion and storage. *Nano Res. Energy* **2022**, *1*, e9120007. [[CrossRef](#)]
6. Tian, Y.D.; Chen, S.; He, Y.L.; Chen, Q.W.; Zhang, L.L.; Zhang, J.T. A highly reversible dendrite-free Zn anode via spontaneous galvanic replacement reaction for advanced zinc-iodine batteries. *Nano Res. Energy* **2022**, *1*, e9120025. [[CrossRef](#)]
7. Sonigara, K.K.; Zhao, J.W.; Machhi, H.K.; Cui, G.L.; Soni, S.S. Self-Assembled Solid-State Gel Catholyte Combating Iodide Diffusion and Self-Discharge for a Stable Flexible Aqueous Zn-I₂ Battery. *Adv. Energy Mater.* **2020**, *10*, 2001997. [[CrossRef](#)]
8. Zhao, J.W.; Li, Y.Q.; Peng, X.; Dong, S.M.; Ma, J.; Cui, G.L.; Chen, L.Q. High-voltage Zn/LiMn_{0.8}Fe_{0.2}PO₄ aqueous rechargeable battery by virtue of “water-in-salt” electrolyte. *Electrochem. Commun.* **2016**, *69*, 6–10. [[CrossRef](#)]
9. Song, M.; Tan, H.; Chao, D.L.; Fan, H.J. Recent Advances in Zn-Ion Batteries. *Adv. Funct. Mater.* **2018**, *28*, 1802564. [[CrossRef](#)]
10. Ma, G.Q.; Miao, L.C.; Dong, Y.; Yuan, W.T.; Nie, X.Y.; Di, S.L.; Wang, Y.Y.; Wang, L.B.; Zhang, N. Reshaping the electrolyte structure and interface chemistry for stable aqueous zinc batteries. *Energy Storage Mater.* **2022**, *47*, 203–210. [[CrossRef](#)]
11. Wang, L.J.; Zhang, Y.; Hu, H.L.; Shi, H.-Y.; Song, Y.; Guo, D.; Liu, X.X.; Sun, X.Q. A Zn(ClO₄)₂ Electrolyte Enabling Long-Life Zinc Metal Electrodes for Rechargeable Aqueous Zinc Batteries. *ACS Appl. Mater. Inter.* **2019**, *11*, 42000–42005. [[CrossRef](#)]
12. Zhan, R.M.; Wang, X.C.; Chen, Z.H.; Seh, Z.W.; Wang, L.; Sun, Y.M. Promises and Challenges of the Practical Implementation of Pre-lithiation in Lithium-Ion Batteries. *Adv. Energy Mater.* **2021**, *11*, 2101565. [[CrossRef](#)]
13. Wang, F.; Borodin, O.; Gao, T.; Fan, X.L.; Sun, W.; Han, F.D.; Faraone, A.; Dura, J.A.; Xu, K.; Wang, C.S. Highly reversible zinc metal anode for aqueous batteries. *Nat. Mater.* **2018**, *17*, 543–549. [[CrossRef](#)]

14. Chao, D.L.; Zhu, C.R.; Song, M.; Liang, P.; Zhang, X.; Tiep, N.H.; Zhao, H.F.; Wang, J.; Wang, R.M.; Zhang, H.; et al. A High-Rate and Stable Quasi-Solid-State Zinc-Ion Battery with Novel 2D Layered Zinc Orthovanadate Array. *Adv. Mater.* **2018**, *30*, 1803181. [[CrossRef](#)]
15. Qiu, H.Y.; Hu, R.X.; Du, X.F.; Chen, Z.; Zhao, J.W.; Lu, G.L.; Jiang, M.F.; Kong, Q.Y.; Yan, Y.Y.; Du, J.Z.; et al. Eutectic Crystallization Activates Solid-State Zinc-Ion Conduction. *Angew. Chem. Int. Ed.* **2022**, *61*, e202113086. [[CrossRef](#)]
16. Han, D.L.; Cui, C.J.; Zhang, K.Y.; Wang, Z.X.; Gao, J.C.; Guo, Y.; Zhang, Z.C.; Wu, S.C.; Weng, Z.; Yang, Q.H.; et al. A non-flammable hydrous organic electrolyte for sustainable zinc batteries. *Nat. Sustain.* **2022**, *5*, 205–213. [[CrossRef](#)]
17. Eng, A.Y.S.; Kumar, V.; Zhang, Y.W.; Luo, J.M.; Wang, W.Y.; Sun, Y.M.; Li, W.Y.; Seh, Z.W. Room-Temperature Sodium–Sulfur Batteries and Beyond: Realizing Practical High Energy Systems through Anode, Cathode, and Electrolyte Engineering. *Adv. Energy Mater.* **2021**, *11*, 2003493. [[CrossRef](#)]
18. Recent Advances and Perspectives for Zn-Based Batteries: Zn Anode and Electrolyte. Available online: https://www.sciopen.com/article/10.26599/NRE.2023.9120039?utm_source=TrendMD&utm_medium=cpc&utm_campaign=Nano_Research_Energy_TrendMD_1 (accessed on 8 November 2022).
19. Mu, Y.L.; Zhou, T.Y.; Zhai, Z.Y.; Zhang, S.B.; Li, D.X.; Chen, L.; Ge, G.L. Metal organic complexes as an artificial solid-electrolyte interface with Zn-ion transfer promotion for long-life zinc metal batteries. *Nanoscale* **2021**, *13*, 20412–20416. [[CrossRef](#)]
20. Wu, K.; Yi, J.; Liu, X.Y.; Sun, Y.; Cui, J.; Xie, Y.H.; Liu, Y.Y.; Xia, Y.Y.; Zhang, J.J. Regulating Zn Deposition via an Artificial Solid-Electrolyte Interface with Aligned Dipoles for Long Life Zn Anode. *Nano-Micro. Lett.* **2021**, *13*, 1–11. [[CrossRef](#)]
21. Toledano, M.; Toledano-Osorio, M.; Hannig, M.; Carrasco-Carmona, Á.; Osorio, M.T.; García-Godoy, F.; Cabello, I.; Osorio, R. Zn-containing Adhesives Facilitate Collagen Protection and Remineralization at the Resin-Dentin Interface: A Narrative Review. *Polymers* **2022**, *14*, 642. [[CrossRef](#)]
22. Hu, J.; Ding, J.W.; Du, Z.G.; Duan, H.P.; Yang, S.B. Zinc anode with artificial solid electrolyte interface for dendrite-free Ni-Zn secondary battery. *J. Colloid Interface Sci.* **2019**, *555*, 174–179. [[CrossRef](#)]
23. Zhao, K.N.; Wang, C.X.; Yu, Y.H.; Yan, M.Y.; Wei, Q.L.; He, P.; Dong, Y.F.; Zhang, Z.Y.; Wang, X.D.; Mai, L.Q. Ultrathin Surface Coating Enables Stabilized Zinc Metal Anode. *Adv. Mater. Interfaces* **2018**, *5*, 1800848. [[CrossRef](#)]
24. Xie, C.L.; Li, Y.H.; Wang, Q.; Sun, D.; Tang, Y.G.; Wang, H.Y. Issues and solutions toward zinc anode in aqueous zinc-ion batteries: A mini review. *Carbon Energy* **2020**, *2*, 540–560. [[CrossRef](#)]
25. Yi, Z.H.; Chen, G.; Hou, F.; Wang, L.; Liang, J. Strategies for the Stabilization of Zn Metal Anodes for Zn-Ion Batteries. *Adv. Energy Mater.* **2020**, *11*, 2003065. [[CrossRef](#)]
26. Hu, W.; Ju, J.G.; Deng, N.P.; Liu, M.Y.; Liu, W.C.; Zhang, Y.X.; Fan, Y.Y.; Kang, W.M.; Cheng, B.W. Recent progress in tackling Zn anode challenges for Zn ion batteries. *J. Mater. Chem. A* **2021**, *9*, 25750–25772. [[CrossRef](#)]
27. Yang, Q.; Li, Q.; Liu, Z.X.; Wang, D.H.; Guo, Y.; Li, X.L.; Tang, Y.C.; Li, H.F.; Dong, B.B.; Zhi, C.Y. Dendrites in Zn-Based Batteries. *Adv. Mater.* **2020**, *32*, 2001854. [[CrossRef](#)]
28. Li, H.F.; Ma, L.T.; Han, C.; Wang, Z.F.; Liu, Z.F.; Tang, Z.J.; Zhi, C.Y. Advanced rechargeable zinc-based batteries: Recent progress and future perspectives. *Nano Energy* **2019**, *62*, 550–587. [[CrossRef](#)]
29. Du, W.C.; Ang, E.H.; Yang, Y.; Zhang, Y.F.; Ye, M.H.; Li, C.C. Challenges in the material and structural design of zinc anode towards high-performance aqueous zinc-ion batteries. *Energy Environ. Sci.* **2020**, *13*, 3330–3360. [[CrossRef](#)]
30. Zhang, T.S.; Tang, Y.; Guo, S.; Cao, X.X.; Pan, A.Q.; Fang, G.Z.; Zhou, J.; Liang, S.Q. Fundamentals and perspectives in developing zinc-ion battery electrolytes: A comprehensive review. *Energy Environ. Sci.* **2020**, *13*, 4625–4665. [[CrossRef](#)]
31. Zhou, J.H.; Xie, M.; Wu, F.; Mei, Y.; Hao, Y.T.; Huang, R.L.; Wei, J.L.; Liu, A.N.; Li, L.; Chen, R.J. Ultrathin Surface Coating of Nitrogen-Doped Graphene Enables Stable Zinc Anodes for Aqueous Zinc-Ion Batteries. *Adv. Mater.* **2021**, *33*, e2101649. [[CrossRef](#)]
32. Lin, H.C.; Jian, Q.F.; Bai, X.Y.; Li, D.Q.; Huang, Z.; Huang, W.T.; Feng, S.S.; Cheng, Z.Y. Recent advances in thermal conductivity and thermal applications of graphene and its derivatives nanofluids. *Appl. Therm. Eng.* **2023**, *218*, 119176. [[CrossRef](#)]
33. Dyck, O.; Yeom, S.; Dillender, S.; Lupini, A.R.; Yoon, M.; Jesse, S. The role of temperature on defect diffusion and nanoscale patterning in graphene. *Carbon* **2023**, *201*, 212–221. [[CrossRef](#)]
34. Nasir, A.; Raza, A.; Tahir, M.; Yasin, T.; Nadeem, M.; Ahmad, B. Synthesis and study of polyaniline grafted graphene oxide nanohybrids. *Mater. Res. Bull.* **2023**, *157*, 112006. [[CrossRef](#)]
35. Low, T.; Chaves, A.; Caldwell, J.; Avouris, P.; Heinz, T.F.; Guinea, F.; Martin-Moreno, L.; Koppens, F. Polaritons in layered two-dimensional materials. *Nat. Mater.* **2017**, *16*, 182–194. [[CrossRef](#)] [[PubMed](#)]
36. Blanc, L.E.; Kundu, D.; Nazar, L.F. Scientific Challenges for the Implementation of Zn-Ion Batteries. *Joule* **2020**, *4*, 771–799. [[CrossRef](#)]
37. Parlak, O.; İncel, A.; Uzun, L.; Turner, A.; Tiwari, A. Structuring Au nanoparticles on two-dimensional MoS₂ nanosheets for electrochemical glucose biosensors. *Biosens. Bioelectron.* **2017**, *89*, 545–550. [[CrossRef](#)]
38. Janowska, I.; Chizari, K.; Ersen, O.; Zafeiratos, S.; Soubane, D.; Costa, V.D.; Speisser, V.; Boeglin, C.; Houllé, M.; Bégin, D.; et al. Microwave synthesis of large few-layer graphene sheets in aqueous solution of ammonia. *Nano Res.* **2010**, *3*, 126–137. [[CrossRef](#)]
39. Safaei, J.; Wang, G.X. Progress and prospects of two-dimensional materials for membrane-based osmotic power generation. *Nano Res. Energy* **2022**, *1*, e9120008. [[CrossRef](#)]
40. Zhang, N.; Chen, X.Y.; Yu, M.; Niu, Z.Q.; Cheng, F.Y.; Chen, J. Materials chemistry for rechargeable zinc-ion batteries. *Chem. Soc. Rev.* **2020**, *49*, 4203–4219. [[CrossRef](#)]
41. Wan, F.; Niu, Z.Q. Design Strategies for Vanadium-based Aqueous Zinc-Ion Batteries. *Angew. Chem. Int. Ed.* **2019**, *58*, 16508–16517. [[CrossRef](#)]
42. Mostafavi, E.; Iravani, S. MXene-Graphene Composites: A Perspective on Biomedical Potentials. *Nano-Micro Lett.* **2022**, *14*, 130. [[CrossRef](#)] [[PubMed](#)]

43. Jia, P.F.; Lu, J.Y.; He, R.F.; Jiang, G.Y.; Jiang, X.; Wang, B.B.; Song, L.; Hu, Y. Octopus sucker-inspired hierarchical structure MXene@carbon nanotubes enhancing the mechanical properties and fire safety of thermoplastic polyurethane composites through the interfacial engineering. *Chem. Eng. J.* **2022**, *450*, 138184. [[CrossRef](#)]
44. Wang, S.; Ma, J.X.; Shi, X.Y.; Zhu, Y.Y.; Wu, Z.S. Recent status and future perspectives of ultracompact and customizable micro-supercapacitors. *Nano Res. Energy* **2022**, *1*, e9120018. [[CrossRef](#)]
45. Zhang, N.N.; Huang, S.; Yuan, Z.S.; Zhu, J.C.; Zhao, Z.F.; Niu, Z.Q. Direct Self-Assembly of MXene on Zn Anodes for Dendrite-Free Aqueous Zinc-Ion Batteries. *Angew. Chem. Int. Ed.* **2021**, *60*, 2861–2865. [[CrossRef](#)] [[PubMed](#)]
46. Park, J.H.; Kwak, M.J.; Hwang, C.; Kang, K.N.; Liu, N.; Jang, J.H.; Grzybowski, B.A. Self-Assembling Films of Covalent Organic Frameworks Enable Long-Term, Efficient Cycling of Zinc-Ion Batteries. *Adv. Mater.* **2021**, *33*, 2101726. [[CrossRef](#)]
47. Cao, J.; Zhang, D.D.; Yue, Y.L.; Wang, X.; Pakornchote, T.; Bovornratanaraks, T.; Zhang, X.Y.; Wu, Z.S.; Qin, J.Q. Oxygen defect enriched $(\text{NH}_4)_2\text{V}_{10}\text{O}_{25}\cdot 8\text{H}_2\text{O}$ nanosheets for superior aqueous zinc-ion batteries. *Nano Energy* **2021**, *84*, 105876. [[CrossRef](#)]
48. Wang, X.; Li, Y.G.; Wang, S.; Zhou, F.; Das, P.; Sun, C.L.; Zheng, S.H.; Wu, Z.S. 2D Amorphous V_2O_5 /Graphene Heterostructures for High-Safety Aqueous Zn-Ion Batteries with Unprecedented Capacity and Ultrahigh Rate Capability. *Adv. Energy Mater.* **2020**, *10*, 2000081. [[CrossRef](#)]
49. Li, Y.; Lu, P.F.; Shang, P.; Wu, L.S.; Wang, X.; Dong, Y.F.; He, R.H.; Wu, Z.S. Pyridinic nitrogen enriched porous carbon derived from bimetal organic frameworks for high capacity zinc ion hybrid capacitors with remarkable rate capability. *J. Energy Chem.* **2021**, *56*, 404–411. [[CrossRef](#)]
50. Dong, Y.F.; Li, Y.; Shi, H.D.; Qin, J.Q.; Zheng, S.H.; He, R.H.; Wu, Z.S. Graphene encapsulated iron nitrides confined in 3D carbon nanosheet frameworks for high-rate lithium ion batteries. *Carbon* **2020**, *159*, 213–220. [[CrossRef](#)]
51. Liu, X.X.; Wei, W.; Yang, Y.F.; Li, Y.J.; Li, Y.; Xu, S.C.; Dong, Y.F.; He, R.H. A porous membrane electrolyte enabled by poly(biphenyl piperidinium triphenylmethane) for dendrite-free zinc anode with enhanced cycling life. *Chem. Eng. J.* **2022**, *437*, 135409. [[CrossRef](#)]
52. Yang, Q.; Li, L.; Hussain, T.; Wang, D.H.; Hui, L.; Guo, Y.; Liang, G.J.; Li, X.L.; Chen, Z.; Huang, Z.D.; et al. Stabilizing Interface pH by N-Modified Graphdiyne for Dendrite-Free and High-Rate Aqueous Zn-Ion Batteries. *Angew. Chem. Int. Ed.* **2022**, *61*, e202112304. [[CrossRef](#)]
53. Wu, L.S.; Zhang, Y.; Shang, P.; Dong, Y.F.; Wu, Z.-S. Redistributing Zn ion flux by bifunctional graphitic carbon nitride nanosheets for dendrite-free zinc metal anodes. *J. Mater. Chem. A* **2021**, *9*, 27408–27414. [[CrossRef](#)]
54. Cao, J.; Zhang, D.D.; Gu, C.; Wang, X.; Wang, S.M.; Zhang, X.Y.; Qin, J.Q.; Wu, Z.S. Manipulating Crystallographic Orientation of Zinc Deposition for Dendrite-free Zinc Ion Batteries. *Adv. Energy Mater.* **2021**, *11*, 2101299. [[CrossRef](#)]
55. Liu, K.; Huang, X.B.; Wang, H.Y.; Li, F.Z.; Tang, Y.G.; Li, J.S.; Shao, M.H. $\text{Co}_3\text{O}_4\text{-CeO}_2/\text{C}$ as a Highly Active Electrocatalyst for Oxygen Reduction Reaction in Al–Air Batteries. *ACS Appl. Mater. Interfaces* **2016**, *8*, 34422–34430. [[CrossRef](#)]
56. Wu, Y.Z.; Liu, S.Q.; Wang, H.Y.; Wang, X.W.; Zhang, X.; Jin, G.H. A novel solvothermal synthesis of Mn_3O_4 /graphene composites for supercapacitors. *Electrochim. Acta.* **2013**, *90*, 210–218. [[CrossRef](#)]
57. Zeng, Y.X.; Lai, Z.Z.; Han, Y.; Zhang, H.Z.; Xie, S.L.; Lu, X.H. Oxygen-Vacancy and Surface Modulation of Ultrathin Nickel Cobaltite Nanosheets as a High-Energy Cathode for Advanced Zn-Ion Batteries. *Adv. Mater.* **2018**, *30*, 1802396. [[CrossRef](#)]
58. Hao, Y.T.; Zhou, J.H.; Wei, G.L.; Liu, A.N.; Zhang, Y.X.; Mei, Y. Artificial N-doped Graphene Protective Layer Enables Stable Zn Anode for Aqueous Zn-ion Batteries. *ACS Appl. Energy Mater.* **2021**, *4*, 6364–6373. [[CrossRef](#)]
59. Li, X.L.; Li, M.; Luo, K.; Hou, Y.; Li, P.; Yang, Q.; Huang, Z.D.; Liang, G.J.; Chen, Z.; Du, S.Y.; et al. Lattice Matching and Halogen Regulation for Synergistically Induced Uniform Zinc Electrodeposition by Halogenated Ti_3C_2 MXenes. *ACS Nano* **2022**, *16*, 813–822. [[CrossRef](#)]
60. Liu, H.Q.; Qiu, M.H.; Tang, C.X.; Xu, J.L.; Jia, H. Enhance interfacial deposition kinetics to achieve dendrite-free zinc anodes by graphene oxide modified boron nitride nanosheets. *Electrochim. Acta.* **2022**, *405*, 139776. [[CrossRef](#)]
61. Zhou, Z.B.; Zhang, Y.M.; Chen, P.; Wu, Y.T.; Yang, H.C.; Ding, H.R.; Zhang, Y.; Wang, Z.Z.; Du, X.; Liu, N. Graphene oxide-modified zinc anode for rechargeable aqueous batteries. *Chem. Eng. Sci.* **2019**, *194*, 142–147. [[CrossRef](#)]
62. Tian, Y.; An, Y.L.; Yang, Y.J.; Xu, B.G. Robust nitrogen/selenium engineered MXene/ZnSe hierarchical multifunctional interfaces for dendrite-free zinc-metal batteries. *Energy Storage Mater.* **2022**, *49*, 122–134. [[CrossRef](#)]
63. Tan, L.W.; Wei, C.L.; Zhang, Y.C.; An, Y.L.; Xiong, S.L.; Feng, J.K. Long-life and dendrite-free zinc metal anode enabled by a flexible, green and self-assembled zincophilic biomass engineered MXene based interface. *Chem. Eng. J.* **2022**, *431*, 134277. [[CrossRef](#)]
64. Wang, N.; Wu, Z.T.; Long, Y.; Chen, D.R.; Geng, C.N.; Liu, X.C. MXene-assisted polymer coating from aqueous monomer solution towards dendrite-free zinc anodes. *J. Energy Chem.* **2022**, *73*, 277–284. [[CrossRef](#)]
65. Zhu, X.D.; Li, X.Y.; Essandoh, M.L.K.; Tan, J.; Cao, Z.Y.; Zhang, X.; Dong, P.; Ajayan, P.M.; Ye, M.X.; Shen, J.F. Interface engineering with zincophilic MXene for regulated deposition of dendrite-free Zn metal anode. *Energy Storage Mater.* **2022**, *50*, 243–251. [[CrossRef](#)]
66. Wu, Y.Z.; Wang, M.C.; Tao, Y.; Zhang, K.; Cai, M.L.; Ding, Y.; Liu, X.P.; Hayat, T.W.; Alsaedi, A.; Dai, S.Y. Electrochemically Derived Graphene-Like Carbon Film as a Superb Substrate for High-Performance Aqueous Zn-Ion Batteries. *Adv. Funct. Mater.* **2019**, *30*, 1907120. [[CrossRef](#)]
67. Bhoyate, S.; Mhin, S.; Jeon, J.E.; Park, K.; Kim, J.; Choi, W. Stable and High-Energy-Density Zn-Ion Rechargeable Batteries Based on a MoS_2 -Coated Zn Anode. *ACS Appl. Mater. Interfaces* **2020**, *12*, 27249–27257. [[CrossRef](#)] [[PubMed](#)]
68. Liu, P.G.; Zhang, Z.Y.; Hao, R.; Huang, Y.P.; Liu, W.F.; Tan, Y.Y.; Li, P.L.; Yan, J.; Liu, K.Y. Ultra-highly stable zinc metal anode via 3D-printed $\text{g-C}_3\text{N}_4$ modulating interface for long life energy storage systems. *Chem. Eng. J.* **2021**, *403*, 126425. [[CrossRef](#)]

69. Manipulating Horizontal Zn Deposition with Graphene Interpenetrated Zn Hybrid Foils for Dendrite-Free Aqueous Zinc Ion Batteries. Available online: <https://onlinelibrary.wiley.com/doi/abs/10.1002/eem2.12423> (accessed on 28 April 2022).
70. Huang, J.H.; Guo, Z.W.; Ma, Y.Y.; Bin, D.; Wang, Y.G.; Xia, Y.Y. Recent Progress of Rechargeable Batteries Using Mild Aqueous Electrolytes. *Small Methods* **2019**, *3*, 1800272. [CrossRef]
71. Konarvo, A.; Voronina, N.; Jo, J.H.; Bakenov, Z.; Sun, Y.K.; Myung, S.T. Present and Future Perspective on Electrode Materials for Rechargeable Zinc-Ion Batteries. *ACS Energy Lett.* **2018**, *3*, 2620–2640. [CrossRef]
72. Fang, G.Z.; Zhou, J.; Pan, A.Q.; Liang, S.Q. Recent Advances in Aqueous Zinc-Ion Batteries. *ACS Energy Lett.* **2018**, *3*, 2480–2501. [CrossRef]
73. Du, W.C.; Huang, S.; Zhang, Y.F.; Ye, M.H.; Li, C.C. Enable commercial Zinc powders for dendrite-free Zinc anode with improved utilization rate by pristine graphene hybridization. *Energy Storage Mater.* **2022**, *45*, 465–473. [CrossRef]
74. Xia, A.L.; Pu, X.M.; Tao, Y.Y.; Liu, H.M.; Wang, Y.G. Graphene oxide spontaneous reduction and self-assembly on the zinc metal surface enabling a dendrite-free anode for long-life zinc rechargeable aqueous batteries. *Appl. Surf. Sci.* **2019**, *481*, 852–859. [CrossRef]
75. Qiu, M.H.; Jia, H.; Liu, H.Q.; Tawiah, B.; Fu, S.H. Realizing Long-life Zn Anode by Few-layer Graphene Ion-oriented Interface. *J. Alloys Compd.* **2022**, *891*, 161886. [CrossRef]
76. Sun, B.; Wang, P.P.; Yang, L.W.; Wei, X.L.; Jin, Y.; Wu, H. Rational Design of an Interfacial Bilayer for Aqueous Dendrite-Free Zinc Anodes. *ACS Appl. Mater. Interfaces* **2022**, *14*, 954–960. [CrossRef]
77. Qiu, M.H.; Wang, D.; Tawiah, B.J.M.; Jia, H.; Fei, B.; Fu, S.H. Constructing PEDOT:PSS/Graphene sheet nanofluidic channels to achieve dendrite-free Zn anode. *Compos. Part B Eng.* **2021**, *215*, 108798. [CrossRef]
78. Gan, H.; Wu, J.; Li, R.; Huang, B.W.; Liu, H.B. Ultra-stable and deeply rechargeable zinc metal anode enabled by a multifunctional protective layer. *Energy Storage Mater.* **2022**, *47*, 602–610. [CrossRef]
79. Zhang, H.; Guo, R.Y.; Li, S.; Liu, C.; Li, H.Y.; Zou, G.Q.; Hu, J.G.; Hou, H.S.; Ji, X.B. Graphene quantum dots enable dendrite-free zinc ion battery. *Nano Energy* **2022**, *92*, 106752. [CrossRef]
80. Tian, Y.; An, Y.L.; Wei, C.L.; Xi, B.J.; Xiong, S.L.; Feng, J.K.; Qian, Y.T. Flexible and Free-Standing $Ti_3C_2T_x$ MXene@Zn Paper for Dendrite-Free Aqueous Zinc Metal Batteries and Nonaqueous Lithium Metal Batteries. *ACS Nano* **2019**, *13*, 11676–11685. [CrossRef]
81. Gu, J.A.; Tao, Y.; Chen, H.; Cao, Z.J.; Zhang, Y.Z.; Du, Z.G.; Cui, Y.L.S.; Yang, S.B. Stress-Release Functional Liquid Metal-MXene Layers toward Dendrite-Free Zinc Metal Anodes. *Adv. Energy Mater.* **2022**, *12*, 2200115. [CrossRef]
82. Gong, Z.; Wang, P.F.; Ye, K.; Zhu, K.; Yan, J.; Wang, G.L.; Chen, G.H.; Cao, D.X. MXene-modified conductive framework as a universal current collector for dendrite-free lithium and zinc metal anode. *J. Colloid. Interface Sci.* **2022**, *625*, 700–710. [CrossRef]
83. Liu, X.Y.; Fang, Y.Z.; Liang, P.C.; Xu, J.H.; Xing, B.; Zhu, K.; Liu, Y.Y.; Zhang, J.J.; Yi, J. Surface-tuned two-dimension MXene scaffold for highly reversible zinc metal anode. *Chin. Chem. Lett.* **2021**, *32*, 2899–2903. [CrossRef]
84. Tian, Y.; An, Y.L.; Liu, C.K.; Xiong, S.L.; Feng, J.K.; Qian, Y.T. Reversible zinc-based anodes enabled by zincophilic antimony engineered MXene for stable and dendrite-free aqueous zinc batteries. *Energy Storage Mater.* **2021**, *41*, 343–353. [CrossRef]
85. An, Y.L.; Tian, Y.; Liu, C.K.; Xiong, S.L.; Feng, J.K.; Qian, Y.T. Rational Design of Sulfur-Doped Three-Dimensional $Ti_3C_2T_x$ MXene/ZnS Heterostructure as Multifunctional Protective Layer for Dendrite-Free Zinc-Ion Batteries. *ACS Nano* **2021**, *15*, 15259–15273. [CrossRef] [PubMed]
86. Zhang, Y.Z.; Cao, Z.J.; Liu, S.J.; Du, Z.G.; Cui, Y.L.S.; Gu, J.A.; Shi, Y.Z.; Li, B.; Yang, S.B. Charge-Enriched Strategy Based on MXene-Based Polypyrrole Layers Toward Dendrite-Free Zinc Metal Anodes. *Adv. Energy Mater.* **2022**, *12*, 2103979. [CrossRef]
87. Jia, H.; Qiu, M.H.; Tang, C.X.; Liu, H.Q.; Fu, S.H.; Zhang, X.W. Nano-scale BN interface for ultra-stable and wide temperature range tolerable Zn anode. *EcoMat* **2022**, *4*, e12190. [CrossRef]
88. Negatively Charged Insulated Boron Nitride Nanofibers Directing Subsurface Zinc Deposition for Dendrite-Free Zinc Anodes. Available online: <https://link.springer.com/article/10.1007/s12274-022-4619-5> (accessed on 15 June 2022).
89. Qiu, M.H.; Jia, H.; Lan, C.T.; Liu, H.Q.; Fu, S.H. An enhanced kinetics and ultra-stable zinc electrode by functionalized boron nitride intermediate layer engineering. *Energy Storage Mater.* **2022**, *45*, 1175–1182. [CrossRef]
90. Yang, Y.; Liu, C.Y.; Lv, Z.H.; Yang, H.; Cheng, X.; Zhang, S.Z.; Ye, M.H.; Zhang, Y.F.; Chen, L.B.; Zhao, J.B.; et al. Redistributing Zn-ion flux by interlayer ion channels in Mg-Al layered double hydroxide-based artificial solid electrolyte interface for ultra-stable and dendrite-free Zn metal anodes. *Energy Storage Mater.* **2021**, *41*, 230–239. [CrossRef]
91. Yin, C.; Zhu, M.; Kong, Y.; Wang, Q.; Zhou, H.H.; Qi, L.M.; Tong, L.M.; Zhang, J. Rapid synthesis of few-layer graphdiyne using radio frequency heating and its application for dendrite-free zinc anodes. *2D Mater.* **2021**, *8*, 044003. [CrossRef]
92. An, G.H.; Hong, J.; Park, S.; Cho, Y.; Lee, S.; Hou, B.; Cha, S.N. 2D Metal Zn Nanostructure Electrodes for High-Performance Zn Ion Supercapacitors. *Adv. Energy Mater.* **2020**, *10*, 1902981. [CrossRef]
93. Cao, Z.J.; Zhang, Y.Z.; Cui, Y.L.S.; Gu, J.N.; Du, Z.G.; Shi, Y.Z.; Shen, K.; Chen, H.; Li, B.; Yang, S.B. Harnessing the Unique Features of 2D Materials toward Dendrite-free Metal Anodes. *Energy Environ. Mater.* **2022**, *5*, 45–67. [CrossRef]
94. Dong, Y.F.; Wu, Z.S.; Ren, W.C.; Cheng, H.M.; Bao, X.H. Graphene: A promising 2D material for electrochemical energy storage. *Sci. Bull.* **2017**, *62*, 724–740. [CrossRef]
95. Khamsanga, S.; Uyama, H.; Nuanwat, W.; Pattananuwat, P. Polypyrrole/reduced graphene oxide composites coated zinc anode with dendrite suppression feature for boosting performances of zinc ion battery. *Sci. Rep.* **2022**, *12*, 8689. [CrossRef] [PubMed]
96. Zhu, X.Q.; Ji, C.C.; Meng, Q.Q.; Mi, H.Y.; Yang, Q.; Li, Z.C.X.; Yang, N.J.; Qiu, J.S. Freeze-Tolerant Hydrogel Electrolyte with High Strength for Stable Operation of Flexible Zinc-Ion Hybrid Supercapacitors. *Small* **2022**, *18*, 2200055. [CrossRef] [PubMed]
97. Zhang, M.H.; Xu, W.; Wu, L.S.; Dong, Y.F. Recent progress in MXene-based nanomaterials for highperformance aqueous zinc-ion hybrid capacitors. *New Carbon Mater.* **2022**, *37*, 508–526. [CrossRef]

98. Liu, F.F.; Jin, S.; Xia, Q.X.; Zhou, A.G.; Fan, L.Z. Research progress on construction and energy storage performance of MXene heterostructures. *J. Energy Chem.* **2021**, *62*, 220–242. [[CrossRef](#)]
99. Dong, Y.F.; Shi, H.D.; Wu, Z.S. Recent Advances and Promise of MXene-Based Nanostructures for High-Performance Metal Ion Batteries. *Adv. Funct. Mater.* **2020**, *30*, 2000706. [[CrossRef](#)]
100. Yang, Q.; Guo, Y.; Yan, B.X.; Wang, C.D.; Liu, Z.X.; Huang, Z.D.; Wang, Y.K.; Li, Y.R.; Li, H.F.; Song, L.; et al. Hydrogen-Substituted Graphdiyne Ion Tunnels Directing Concentration Redistribution for Commercial-Grade Dendrite-Free Zinc Anodes. *Adv. Mater.* **2020**, *32*, 2001755. [[CrossRef](#)]
101. He, H.B.; Tong, H.; Song, X.Y.; Song, X.P.; Liu, J. Highly stable Zn metal anodes enabled by atomic layer deposited Al₂O₃ coating for aqueous zinc-ion batteries. *J. Mater. Chem. A* **2020**, *8*, 7836–7846. [[CrossRef](#)]
102. Gómez, I.J.; Alegret, N.; Dominguez-Alfaro, A.; Vázquez Sulleiro, M. Recent Advances on 2D Materials towards 3D Printing. *Chemistry* **2021**, *3*, 1314–1343. [[CrossRef](#)]
103. Yang, R.; Zhou, J.Z.; Yang, C.; Qiu, L.; Cheng, H.M. Recent Progress in 3D Printing of 2D Material-Based Macrostructures. *Adv. Mater. Technol.* **2020**, *5*, 1901066. [[CrossRef](#)]
104. Zheng, J.X.; Huang, Z.H.; Zeng, Y.; Liu, W.Q.; Wei, B.B.; Qi, Z.B.; Wang, Z.C.; Xia, C.; Liang, H.F. Electrostatic Shielding Regulation of Magnetron Sputtered Al-Based Alloy Protective Coatings Enables Highly Reversible Zinc Anodes. *Nano Lett.* **2022**, *22*, 1017–1023. [[CrossRef](#)] [[PubMed](#)]